Eleventh US-Japan Workshop
On Heavy Ion Fusion and High Energy Density Physics

Friday, 19 December 2008
Grand Canyon Room, B543
Lawrence Livermore National Laboratory,
Livermore, CA, USA

Energy Deposition Profile of Heavy-Ions in Warm Dense Targets

Yoshiyuki Oguri

Research Laboratory for Nuclear Reactors,
Tokyo Institute of Technology (Tokyo Tech)

Pulsed heavy-ion beams are one of the options to produce “Warm Dense Matter (WDM)” in laboratories.

- Ion-driven WDM facility planned by US-HIFS-VNL[1]:
  - Sub-range solid target → Homogeneous heating using the “Bragg peak”
  - ≈ 1 MeV/u heavy projectiles → Moderate cost
- However, the Bragg curve shape can change during irradiation by
  - increase of temperature
  - decrease of density (if hydro expansion is not negligible).

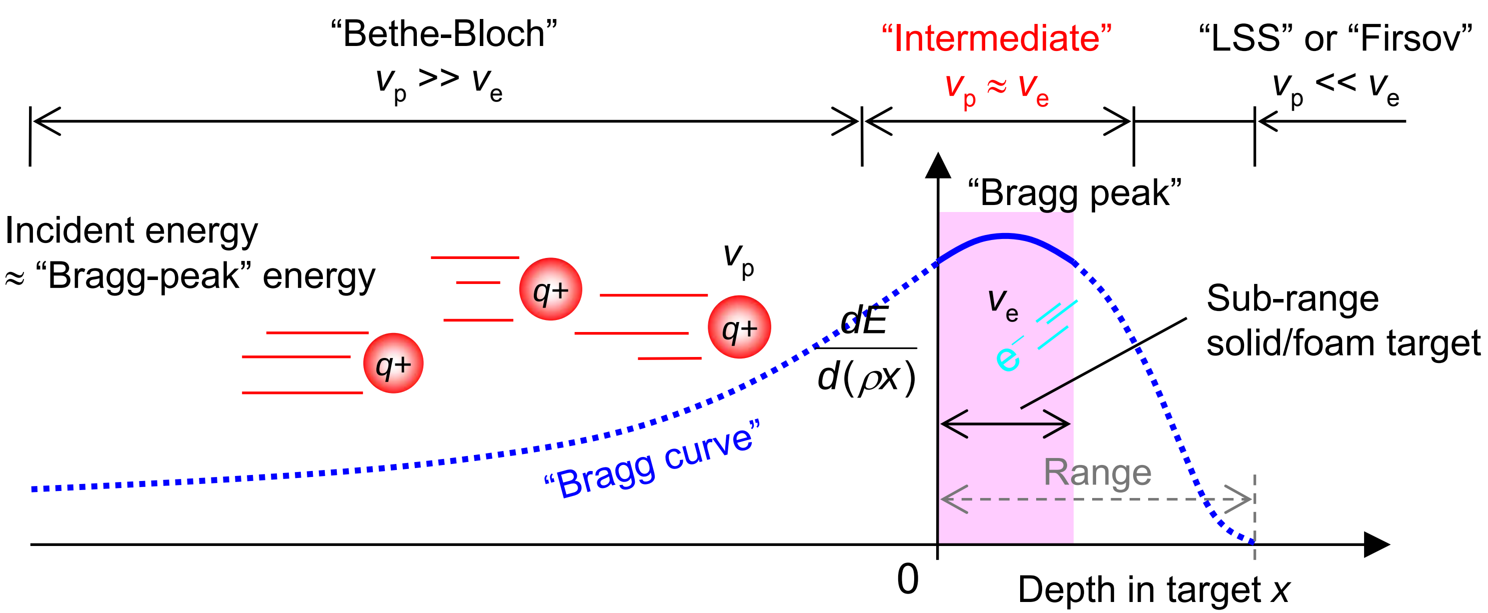

[1]B. G. Logan, *"Progress of heavy ion fusion science towards warm dense matter physics"*, Workshop on accelerator driven warm dense matter physics, Pleasanton, CA, February 22-24, 2006.

Objective: To investigate the change of energy deposition profile in sub-range targets during irradiation

- Requirements for the *dE/dx* calculation:
  - Stopping power in targets with a given temperature and a given density must be evaluated.
    → Not very precise, but robust approach is needed.
  - Intermediate velocity around the Bragg peak ($v_p \approx v_e$)
    → Neither Bethe ($v_p >> v_e$)-, nor LSS/Firsov ($v_p << v_e$) approaches can be applied.
    → More general method must be employed.
  - Heating starts from room temperature and solid-state (or foam) density.
    → Numerical results must be consistent with those on well-established stopping power data for cold matter, such as SRIM[2].
- Main issues:
  - Calculation with beam- and target parameters inspired by a VNL future scenario[3]:
    - ${}^{23}_{11}$Na projectile; ≈ 1 MeV/u, ≈ 1 GW/mm^2, ≈ 1 ns
    - ${}^{27}_{13}$Al target; 1-100% solid density
  - Coupling with a hydrodynamic code

[2] J. F. Ziegler and J. P. Biersack, *"Computer Code SRIM2006"*, United States Naval Academy, Annapolis, MD, http://www.srim.org (2006).

A straightforward approach[3] was applied to calculate the electronic stopping power near the Bragg peak.

- The target atom was divided into many shells, and contribution of each shell was added to calculate the total stopping power:
  - Electronic stopping cross section S_e was calculated by integrating differential scattering cross section $d\sigma/d(\delta E)$ over all possible energy transfer:

$$S_e = 4\pi \int_0^{R_{WS}} \int_0^{\infty} \left\{ \int_{\delta E_{min}}^{\delta E_{max}} \delta E \frac{d\sigma}{d(\delta E)} (1-g) d(\delta E) \right\} \Bigg|_{r, v_e} f_e(r, v_e) dv_e r^2 dr,$$

improved since HIF2008!

R_{WS}	: Wigner-Seitz radius $R_{WS} = (3n_{atom}/4\pi)^{1/3}$
δE	: Energy transfer by a projectile-electron collision
δE_{min}	: Minimum energy transfer
δE_{max}	: Maximum energy transfer
$f_e(r,v_e)$	: Electron density distribution in phase space
g	: Final state ($v_e = v_e'$) occupation

  - Finite temperature Thomas-Fermi model:

$$f_e(r, v_e) \equiv \left(\frac{1}{m_e \pi^2 \hbar^3} \right) \frac{1}{1 + \exp\left(\dfrac{m_e v_e^2/2 - e\phi(r) - E_F}{kT} \right)}.$$

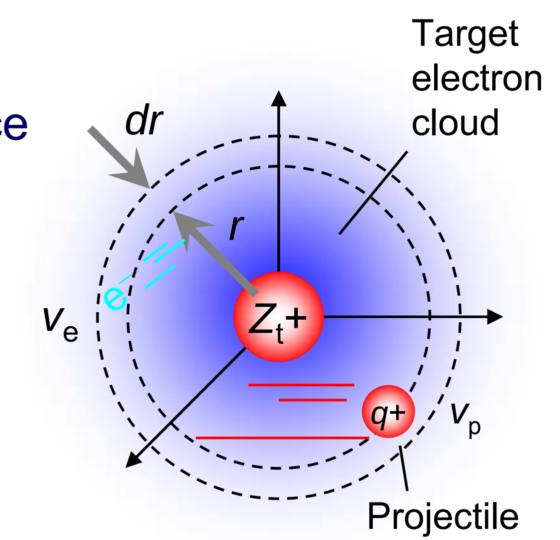

[3]E. Kührt and R. Wedell, *Phys. Lett.* **86 A** (1981) 54.

To take into account the target electron motion, a classical collisional model was employed.

- The projectile and the target electrons were assumed to be point charges:
  - Differential scattering cross section[4] corresponding to an energy transfer δE for isotropic electron velocity distribution:

$$\frac{d\sigma}{d(\delta E)} = \frac{\pi}{3}\frac{q^2 e^4}{(4\pi\varepsilon_0)^2 v_p} \times F$$

$$F \equiv 3v_e'^2 - v_e^2 \quad \text{for } 0 < \delta E \le \delta E^*$$

$$\equiv \frac{(v_p' + v_p)^3 + (v_e' - v_e)^3}{2v_e} \quad \text{for } \delta E^* \le \delta E < \delta E_{max}$$

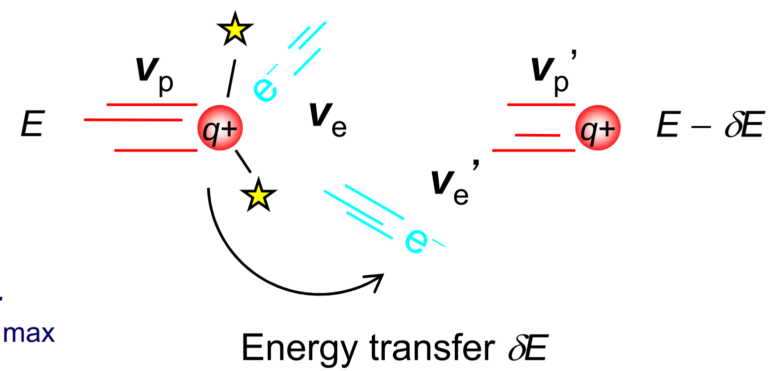

  - Maximum energy transfer:

$$\delta E_{max} \equiv 2m_e v_p (v_p + v_e) \qquad \left(\delta E^* \equiv 2m_e v_p (v_p - v_e)\right)$$

  - Velocities after the collision:

$$v_p' \equiv \sqrt{v_p^2 - \frac{2\delta E}{m_p}}, \quad v_e' \equiv \sqrt{v_e^2 + \frac{2\delta E}{m_e}},$$

[4]E. Gerjuoy, *Phys. Rev.* **148** (1966) 54.

Minimum energy transfer δE_{min} at each shell was determined by "Local plasma approximation (LPA)".

- Electron cloud around the nucleus = electron gas ≈ inhomogeneous plasma:
  - $\delta E_{\mathrm{min}} \approx$ Local plasmon energy = $\gamma\hbar\omega_{\mathrm{p}}(r)$ (γ: Correction factor ≈ $\sqrt{2}$)
  - Local plasma frequency $\omega_{\mathrm{p}}(\boldsymbol{r}) = \sqrt{\dfrac{e^2 n_{\mathrm{e}}(\boldsymbol{r})}{\varepsilon_0 m_{\mathrm{e}}}}$, $n_{\mathrm{e}}(\boldsymbol{r}) = n_{\mathrm{eb}}(\boldsymbol{r}) + n_{\mathrm{ef}}(\boldsymbol{r})$
- Fermi-degeneracy due to the strong coupling was taken into account for the scattering cross section:
  - Pauli-exclusion due to Fermi-degeneracy
    $\rightarrow$ Effective scattering cross section
    $\propto$ Vacancy of the final state
    = 1 – Occupation = 1 – g
  - Fermi-Dirac occupation function:

$$g(r, v_{\mathrm{e}}') \equiv \frac{1}{1 + \exp\left(\dfrac{m_{\mathrm{e}} v_{\mathrm{e}}'^2/2 - e\phi(r) - E_{\mathrm{F}}}{kT}\right)}$$

v_{e}': Electron velocity after collision
$\phi(r)$: Electrostatic potential, E_{F}: Fermi energy

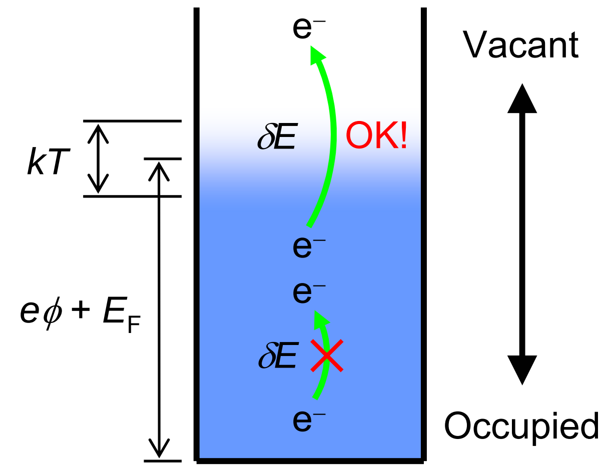

Distribution of target electron velocity was taken into account also in the projectile charge calculation.

- Projectile charge q was determined by relative velocity between the projectile and target electrons:

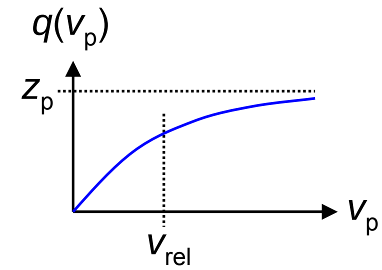

$$q(r) = z_\mathrm{p}\left\{1 - \exp\left(-\frac{v_\mathrm{p}}{v_\mathrm{rel}(r)}\right)\right\}$$

  - Averaged relative velocity for isotropic electron motion:

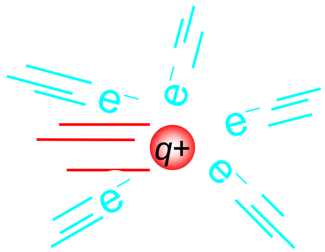

$$v_\mathrm{rel}(r) \equiv \frac{\left(v_\mathrm{p} + \langle v_\mathrm{e}(r)\rangle\right)^3 - \left|v_\mathrm{p} - \langle v_\mathrm{e}(r)\rangle\right|^3}{6 v_\mathrm{p} v_\mathrm{e}(r)}$$

- Nuclear stopping[5] was included to calculate the total stopping cross section:
  - Total stopping S_calc = Electronic stopping S_e + Nuclear stopping S_n*:

$$S_\mathrm{n} = \frac{s_\mathrm{n}(8.462 z_\mathrm{p} Z_\mathrm{t} A_\mathrm{p})}{(A_\mathrm{p} + A_\mathrm{t})\sqrt{z_\mathrm{p}^{2/3} + Z_\mathrm{t}^{2/3}}}$$

$$s_\mathrm{n} \equiv \frac{0.5\ln(1+\varepsilon)}{(\varepsilon + 0.10718\varepsilon^{0.37544})}, \quad \varepsilon \equiv \frac{32.53 A_\mathrm{t} E}{z_\mathrm{p} Z_\mathrm{t}(A_\mathrm{p} + A_\mathrm{t})\sqrt{z_\mathrm{p}^{2/3} + Z_\mathrm{t}^{2/3}}} \quad (E \text{ in keV}, A \text{ in amu})$$

[5] J. F. Ziegler, *"Handbook of Stopping Cross Sections for Energetic Ions in All Elements"*, Pergamon Press, ISBN 0-08-021607-2 (1980) .

When the target is heated isometrically, electrons move to outer shells, and are excited to high velocities.

- Temperature-dependence of $n_e(r)$ and $\langle v_e(r) \rangle$ in an $_{13}$Al target atom at constant target density $\rho = 0.01\rho_{solid}$:

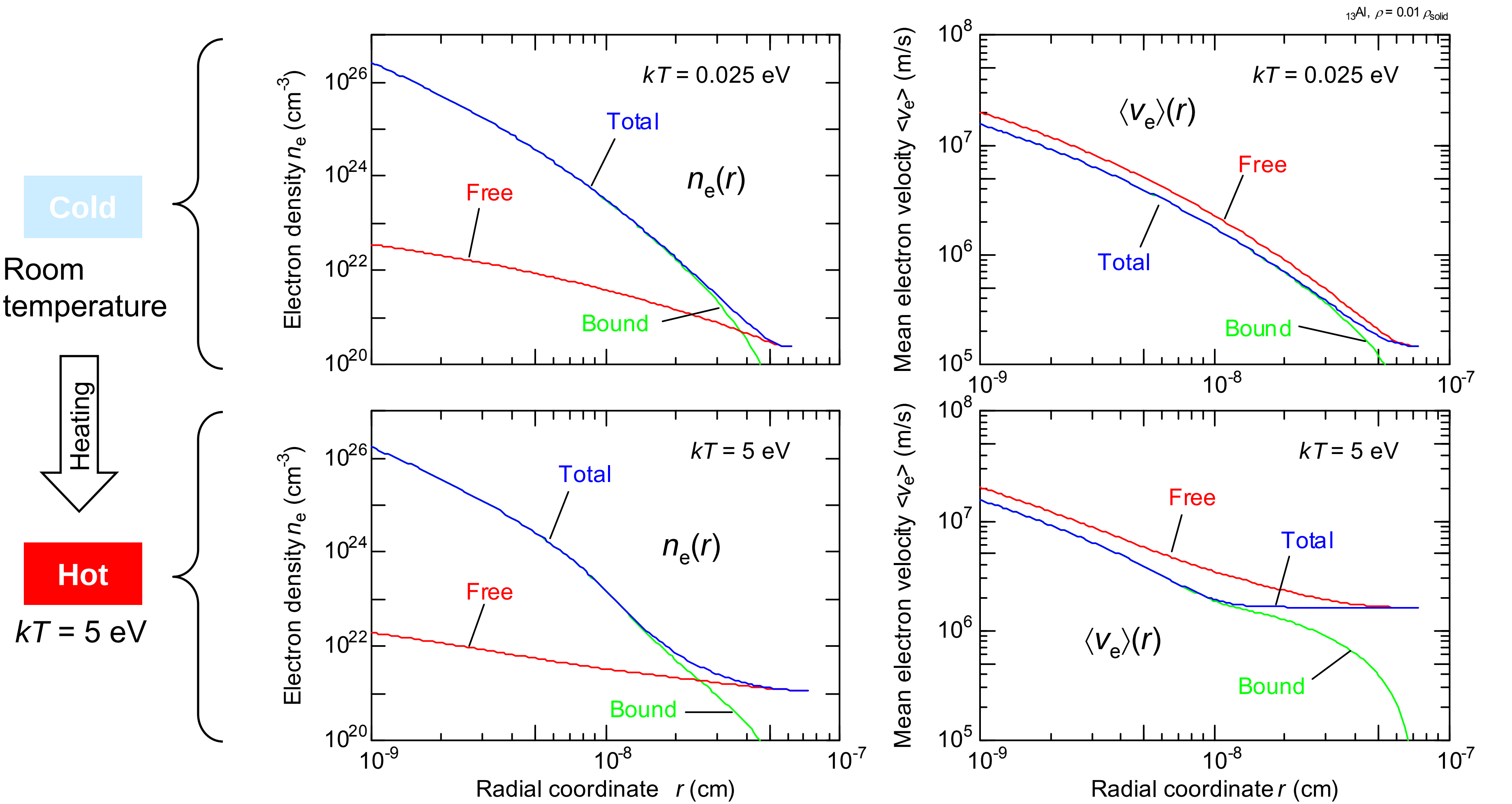

If the target expands isothermally, thermal ionization occurs at outer atomic shells.

- Density-dependence of $n_e(r)$ and $\langle v_e(r) \rangle$ in an $_{13}$Al target atom at constant target temperature $kT = 4$ eV:

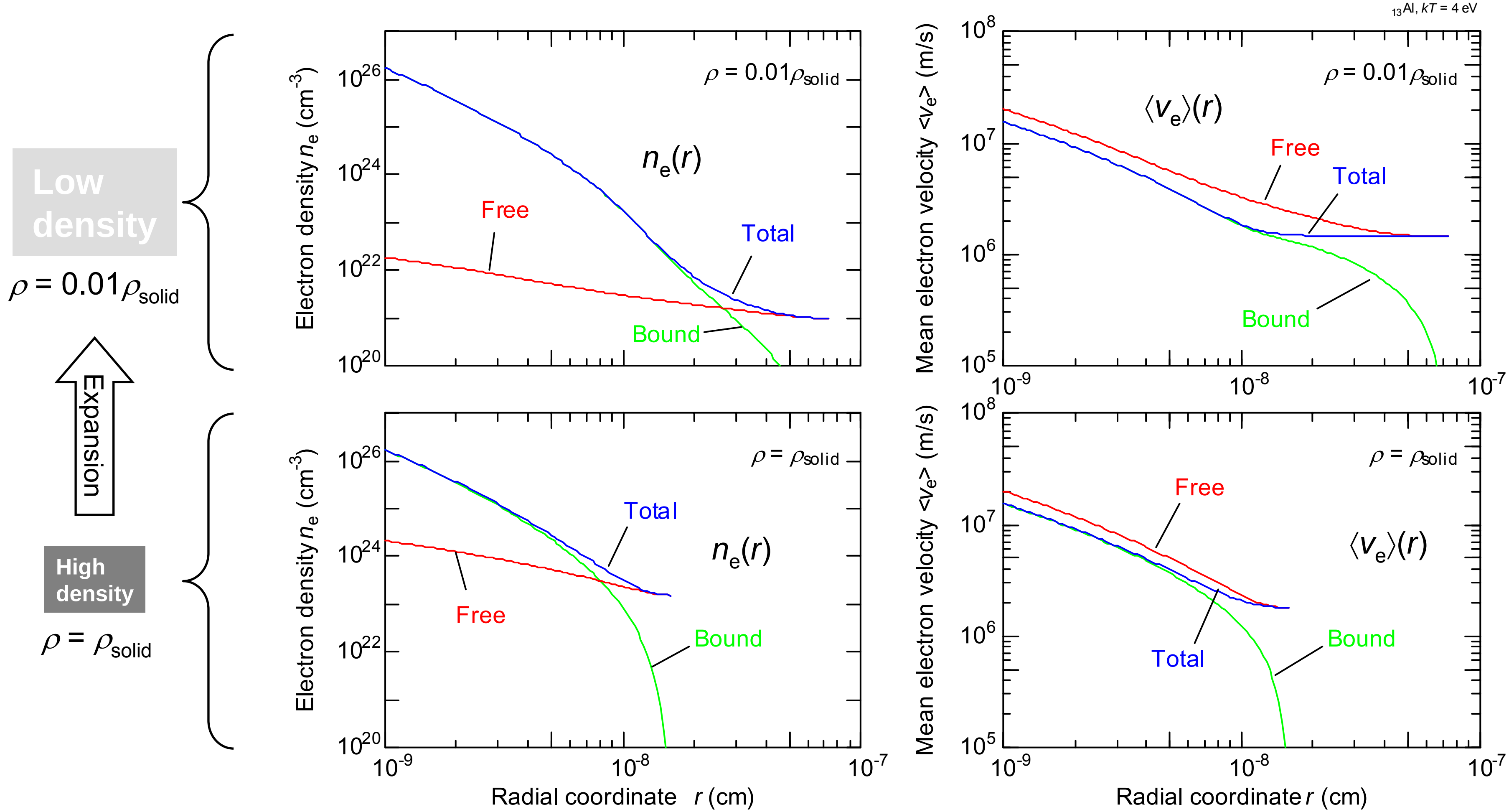

For the cold solid target, shape of the calculated Bragg curve agrees well with that on established databases[2,7].

- Bragg curve for $_{11}$Na projectiles in a solid, room-temperature $_{13}$Al target:
  - The absolute value S was evaluated by adjusting S_{calc} with "projectile fractional effective charge"[5] $z_p^* \equiv \sqrt{\frac{S_{\mathrm{exp}}}{S_{\mathrm{calc}}}}$ (≈ 1.15).

$$S = z_p^{*2} S_{\mathrm{calc}}$$

($dE/dx = S \times$ number density of target atoms)

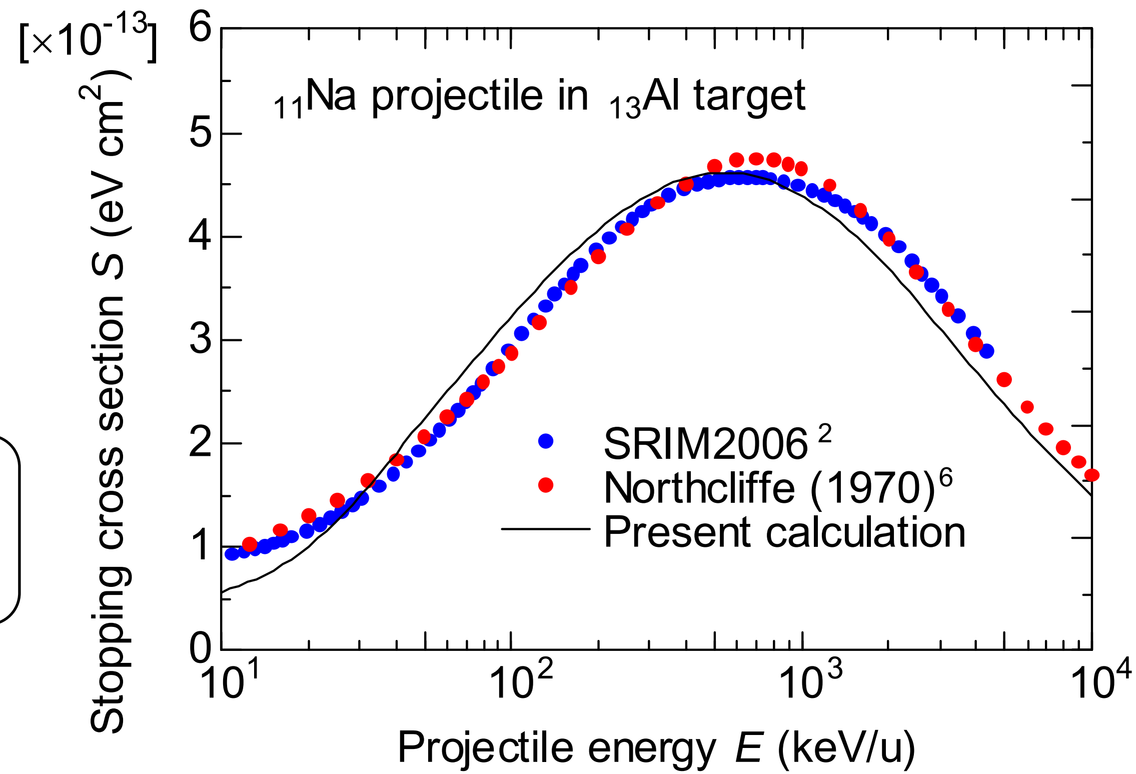

[6]L. C. Northcliffe and R. F. Schilling, *Nucl. Data Tables* **A7** (1970) 233.

Owing to recent improvement, unreasonable sharp peaks due to free electrons disappeared.

- Cf. improvement from previous results presented at HIF2008:
  - Previous (HIF2008): $S_{\mathrm{e}} = 4\pi \int_0^{R_{\mathrm{WS}}} \left\{ \int_{\delta E_{\min}}^{\delta E_{\max}} \delta E \frac{d\sigma}{d(\delta E)} (1-g) d(\delta E) \right\} \bigg|_r n_{\mathrm{e}}(r) r^2 dr.$
  - Present: $S_{\mathrm{e}} = 4\pi \int_0^{R_{\mathrm{WS}}} \int_0^{\infty} \left\{ \int_{\delta E_{\min}}^{\delta E_{\max}} \delta E \frac{d\sigma}{d(\delta E)} (1-g) d(\delta E) \right\} \bigg|_{r, v_{\mathrm{e}}} f_{\mathrm{e}}(r, v_{\mathrm{e}}) dv_{\mathrm{e}} r^2 dr.$

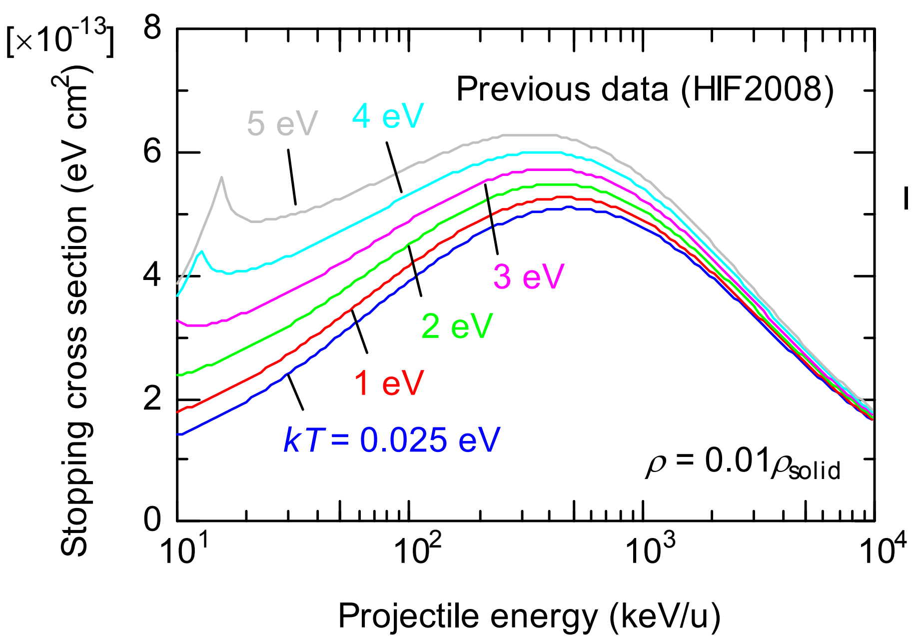

Improvement

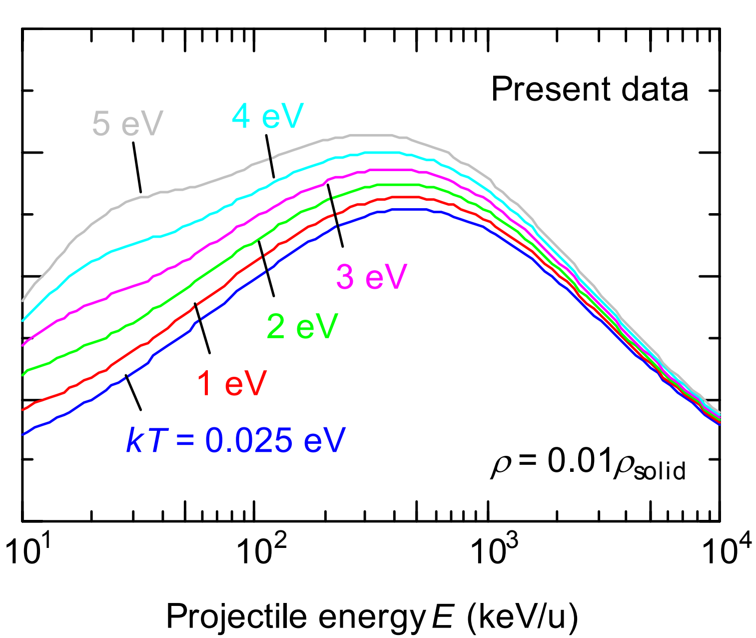

Shape of the Bragg curve changes with target temperature, especially at low densities.

- When the target temperature increases by irradiation,
  - the Bragg peak moves to the low-energy side,
  - stopping power increases especially at low projectile energies,
  - a satellite peak appears owing to energy transfer to free electrons.
- Very small change for solid density target.

High density

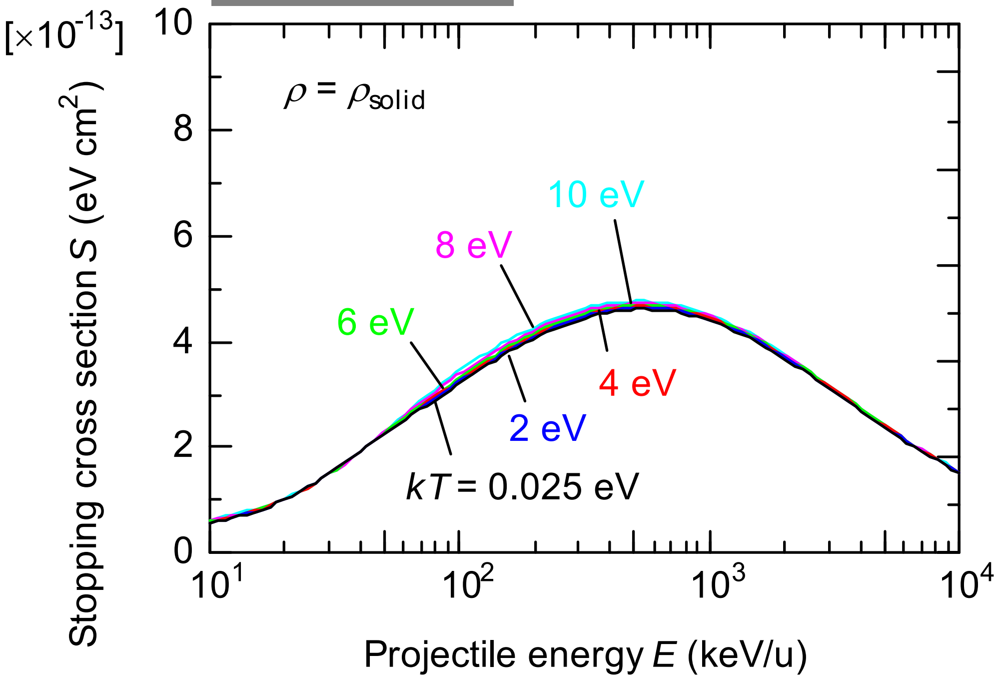

Low density

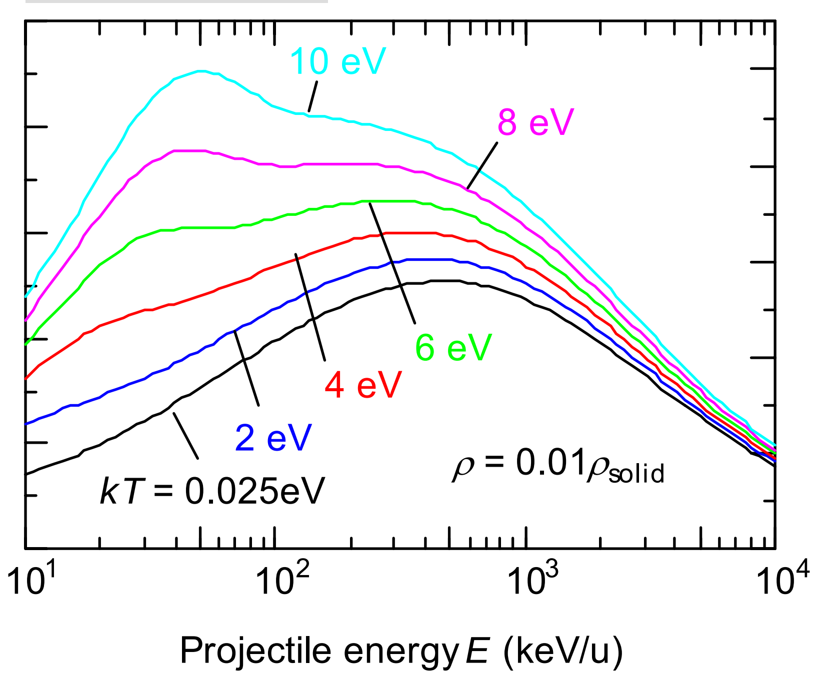

Shape of the Bragg curve changes also with target density, especially at high temperatures.

- When the target density is decreased,
  - the Bragg peak moves towards the low-energy side,
  - stopping power increases especially at low projectile energies,
  - a satellite peak appears owing to energy transfer to free electrons.
- At the room temperature, saturation of $dE/d(\rho x)$ is observed for $\rho < 0.01\rho_{solid}$.

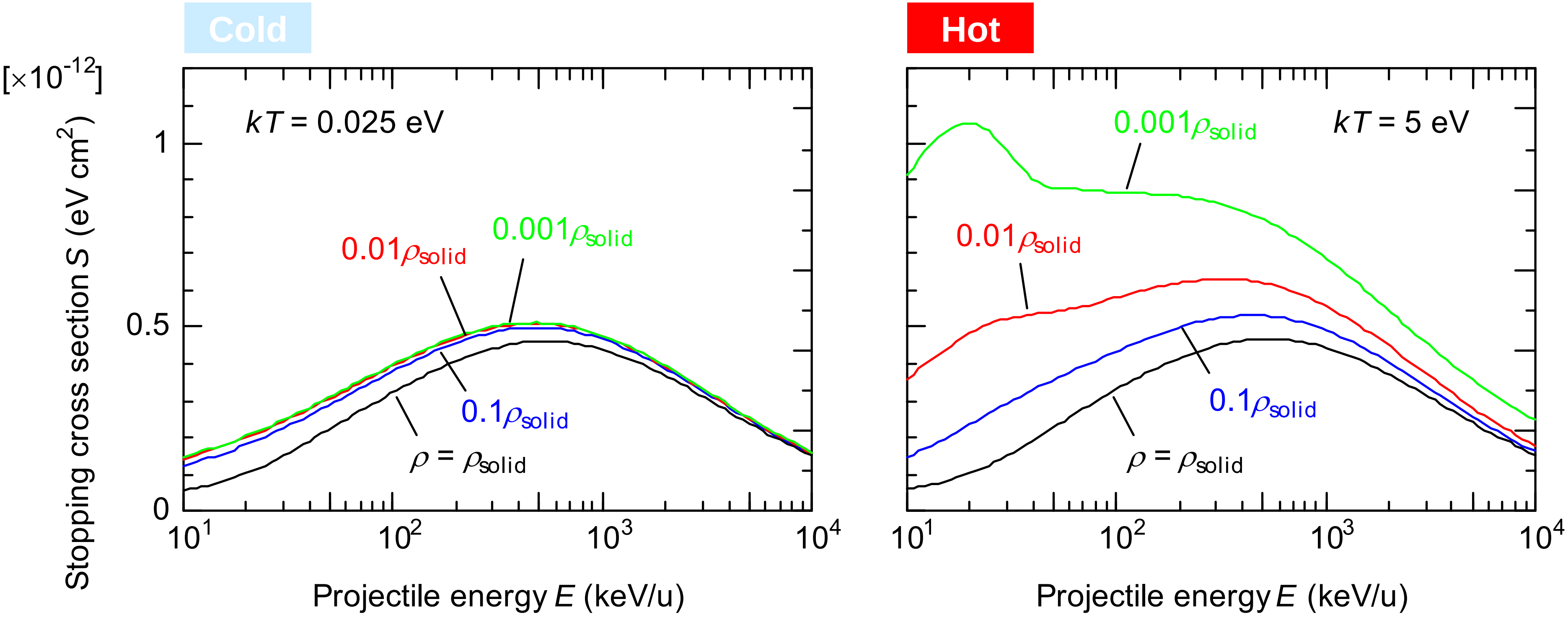

Using the evaluated *dE/dx* data, energy deposition profile during heating was calculated.

- A demonstrative example (not so far away from the VNL future scenario[1]):
  - Projectile: 29.2-MeV $^{23}Na^{+}$ (1.27 MeV/u), 8 GW/mm^2 (peak) × 1 ns
    → Energy per pulse W = 8 J/mm^2 (1.7×10^{13} ions/mm^2)
  - Target: $_{13}$Al-slab, ρ = 1.00-0.01ρ_{solid}, thickness = 9.15-915 μm
  - $dE/d(\rho x)$-inhomogeneity = ± 5%, if cold solid data are used.

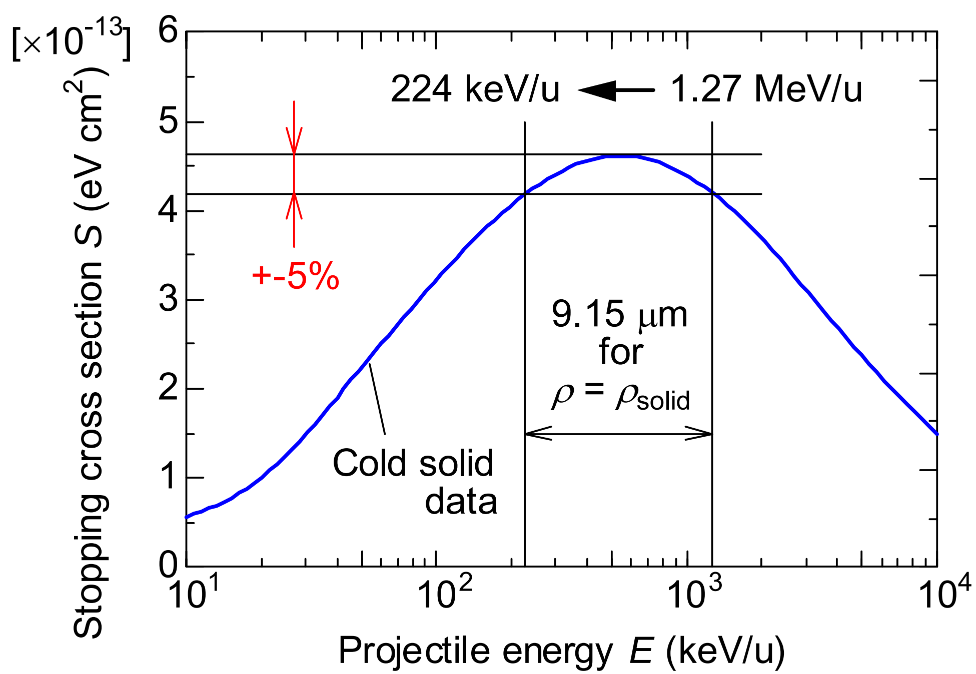

Density (ρ/ρ_{solid})	1	0.1	0.01
Thickness (μm)	9.15	91.5	915

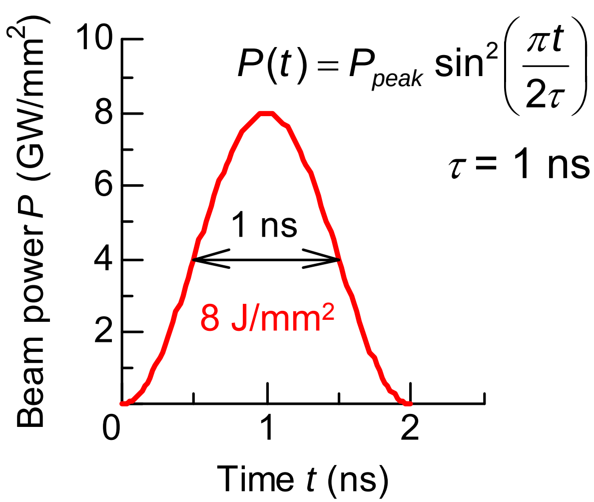

Hydro motion of the target was analyzed using a 1D code being coupled with the *dE/dx* data.

- Original hydro code summary:
  - "MULTI (MULTIgroup radiation transport in MULTIlayer foils)"[7], version 7 by Rafael Ramis (MPQ, Garching)
  - 1D radiation hydrodynamics
  - Fully implicit Lagrangian scheme
  - Time-splitting algorithm
  - Tabulated EOS data (SESAME table)
- Modifications made by this work:
  - Laser deposition routine was canceled.
  - Original ion beam deposition routine (constant *dE/dx*!) was modified to use a *dE/dx* (E,ρ,kT) table ("WDM data") prepared by the present methods.
  - Heat conductivity: Classical heat flux by Spitzer $\rightarrow$ SESAME table
  - FORTRAN77 source code was modified for Windows® machines $\rightarrow$ Typical running time $\approx$ 10 min (Pentium® 4)

[7]R. Ramis, R. Schmalz and J. Mayer-ter-Vehn, *Computer Physics Communications* **49** (1988) 475.

If a thin solid target is used, target expansion during irradiation is too much to obtain well-defined state.

- Streak image of Lagrangian fluid element positions for $\rho = \rho_{solid}$ target:
  - Expansion is slightly asymmetric owing to the energy deposition profile.
  - Almost same hydrodynamic behaviors are observed for both calculations.

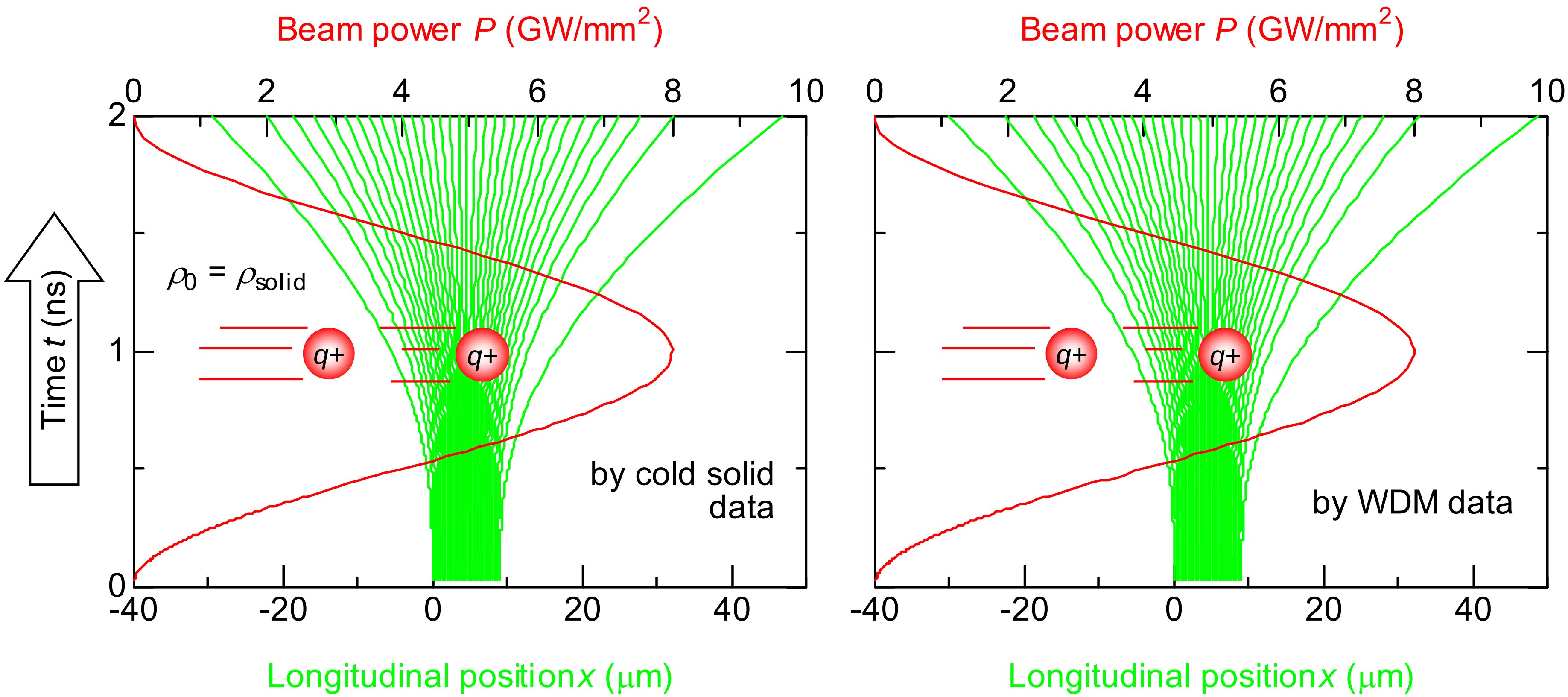

At the end of the irradiation, expansion of the target is not acceptable for WDM research.

- Snapshot of depth profile of parameters at t = 2.0 ns (end of the pulse):
  - Solid lines with WDM data by this work, broken lines with cold solid data
  - The averaged density decreased from ρ_{solid} to $\approx 0.12\rho_{solid}$.
  - Specific energy deposition ($dE/(\rho dx)$) increased due to temperature rise.
  - Both surface layers were strongly heated owing to the decrease of density.
    $\rightarrow$ Energy-deposition inhomogeneity = ±5% (designed) $\rightarrow$ ±13%

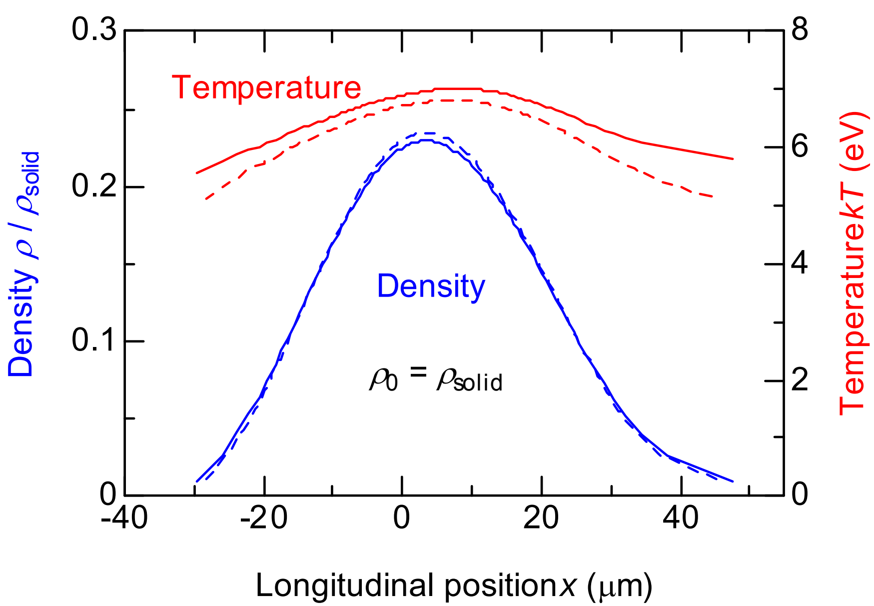

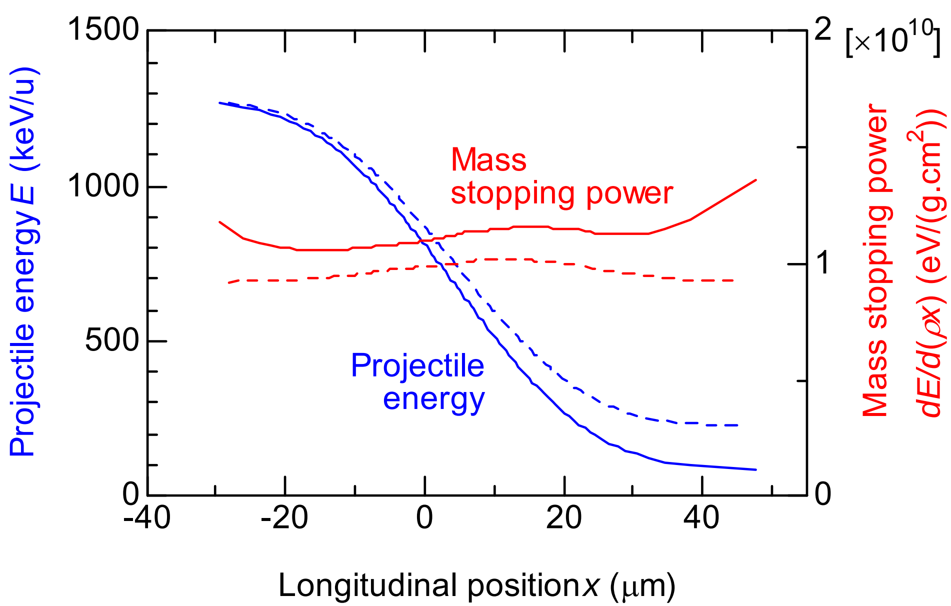

For intermediate-thickness target, rarefaction wave does not reach the center of the target during irradiation.

- Streak image of Lagrangian fluid element positions for $\rho = 0.1\rho_{solid}$ target:
  - Solid lines with WDM data, broken lines with cold solid data
  - Sound speed $c_s = \{\gamma(\gamma-1)U/\rho\}^{1/2} \approx 2\times10^6$ cm/s, Pulse duration $\approx \tau = 1$ ns
    $\rightarrow$ Propagation distance $c_s\tau \approx 20$ μm < Target thickness 91.5 μm

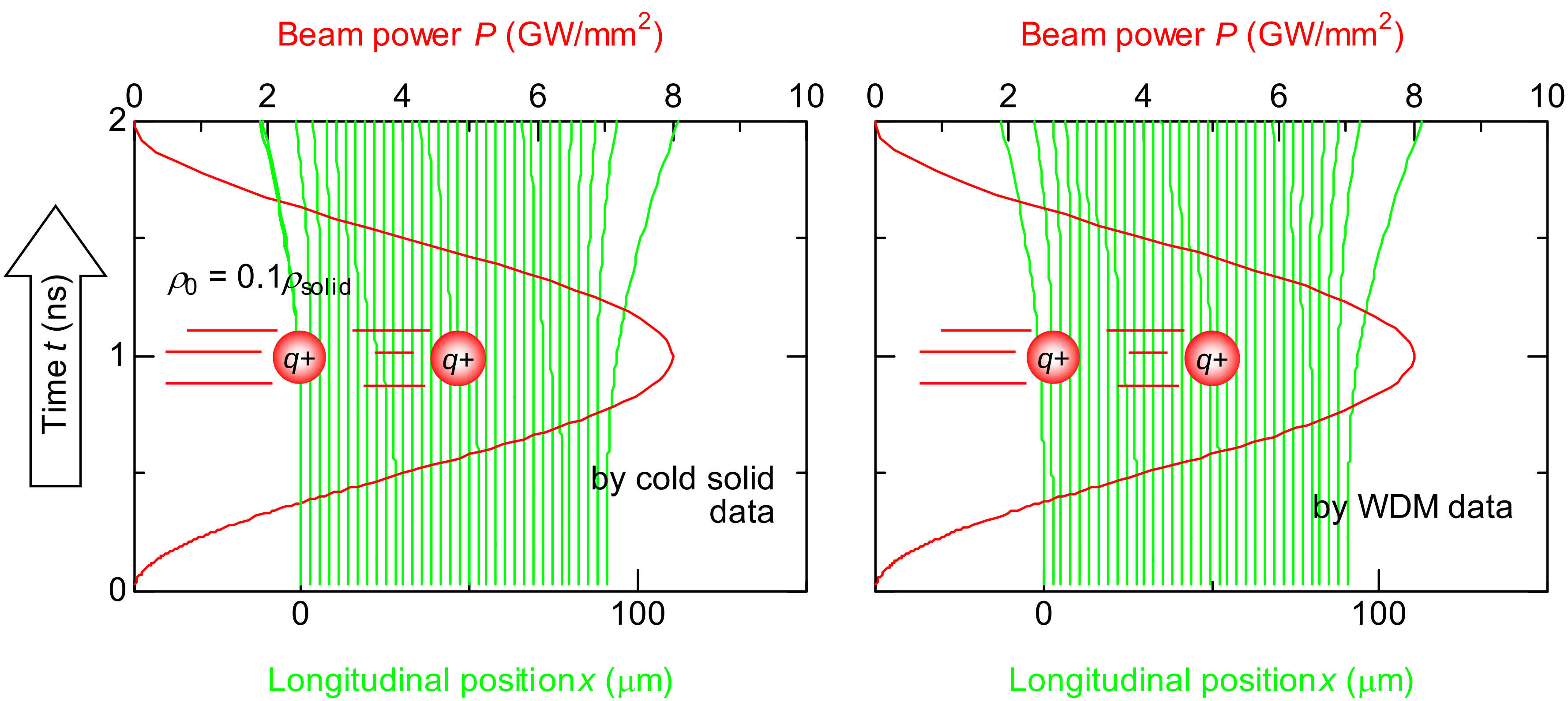

Owing to the increase of *dE/dx* with temperature, the exit energy decreased down to ≈ 0.

- Snapshot of depth profile of parameters at t = 2.0 ns (end of the pulse):
  - Solid lines with WDM data, broken lines with cold solid data
  - Homogeneous density- and temperature profile are obtained only in the center region.
  - Owing to the change of the Bragg curve shape, the energy deposition inhomogeneity increased up to ±15% at the end of the pulse.

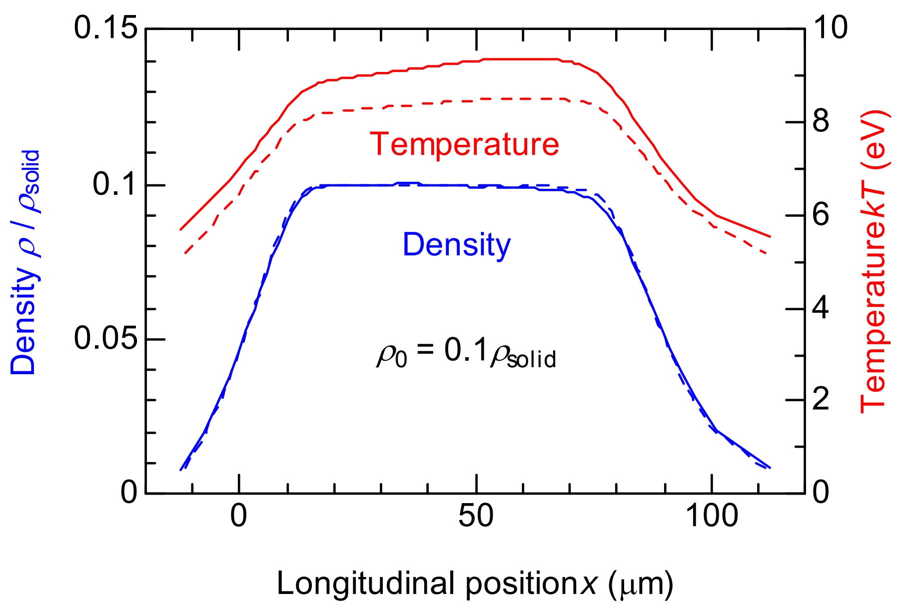

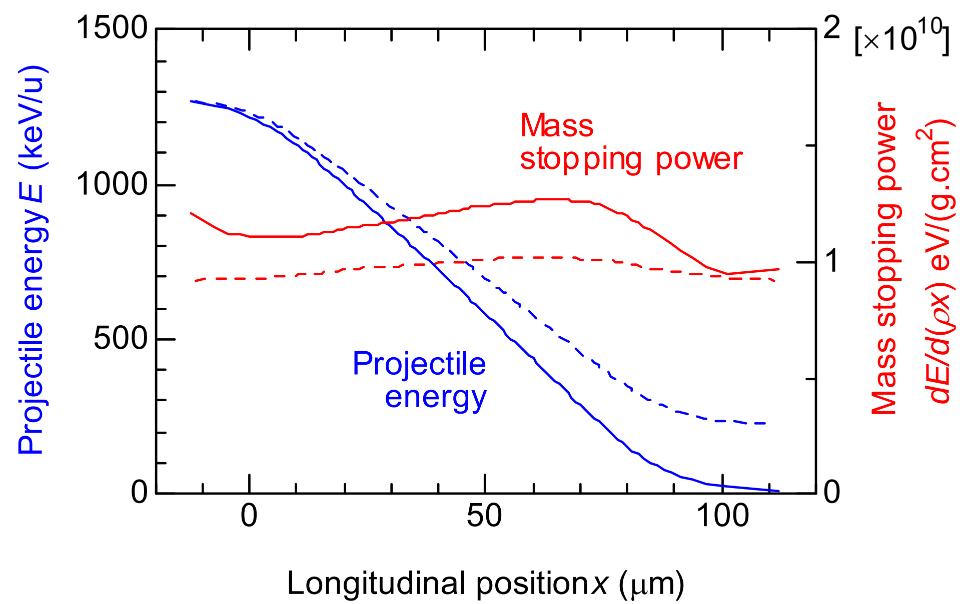

Almost no hydrodynamic motion was observed for the low-density thick target.

- Streak image of Lagrangian fluid element positions for $\rho = 0.01\rho_{solid}$ target:
  - Propagation distance of the rarefaction wave during heating

$$c_s\tau \approx 20\ \mu\text{m} << \text{Target thickness } 915\ \mu\text{m}$$

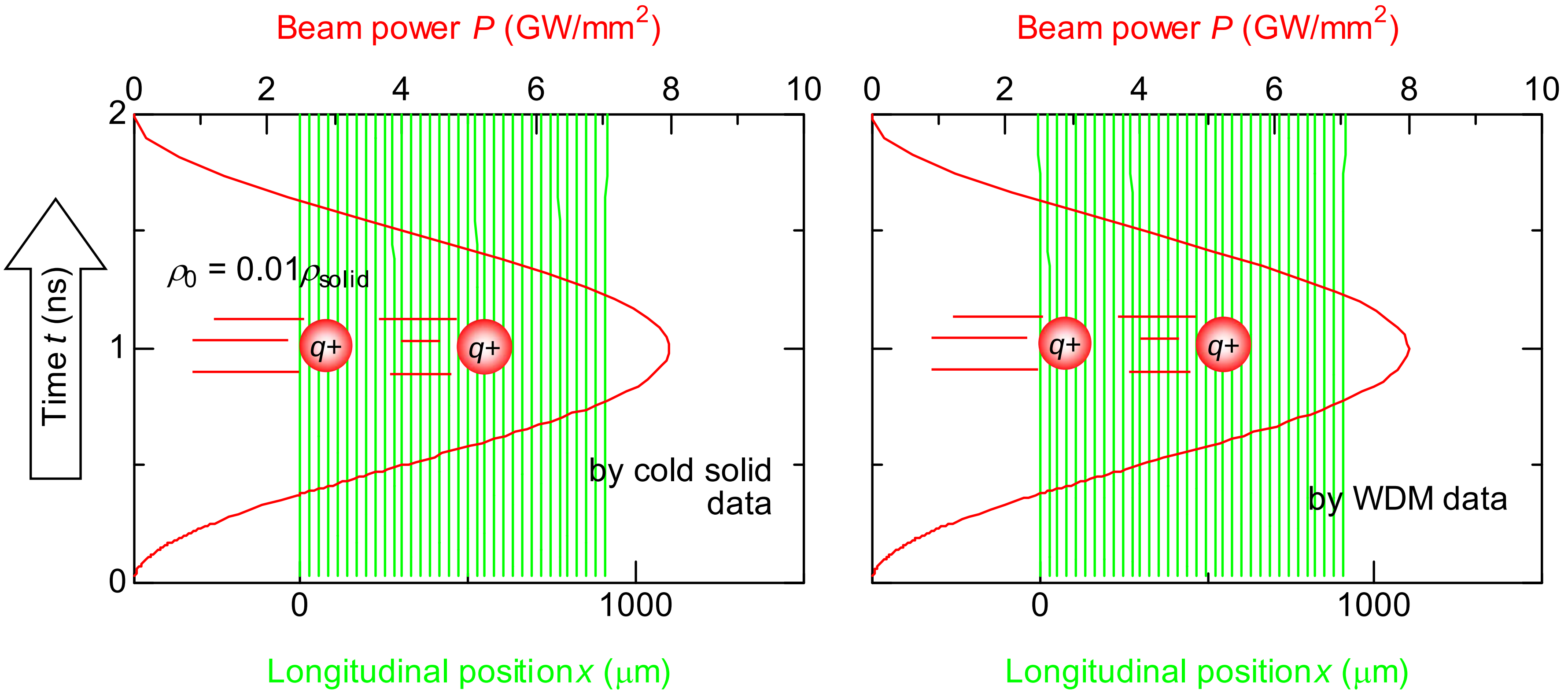

Energy deposition profile in the thick foam target is strongly affected by the change of Bragg-curve shape.

- Snapshot of depth profile of parameters at t = 2.0 ns (end of the pulse):
  - Solid lines with WDM data, broken lines with cold solid data
  - The temperature profile shows a linear decrease near the rear surface.
  - At the end of the pulse the projectile stops in the target due to the increase of stopping power.

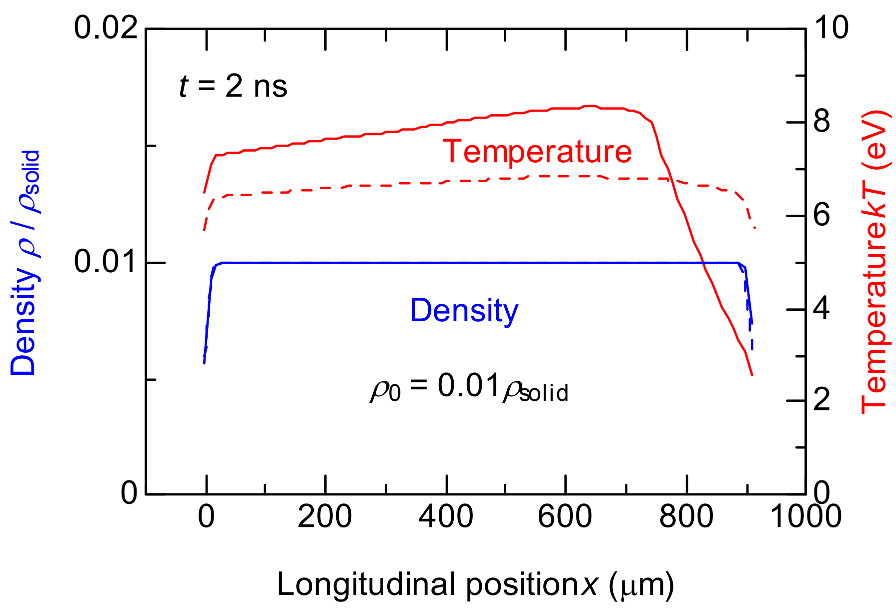

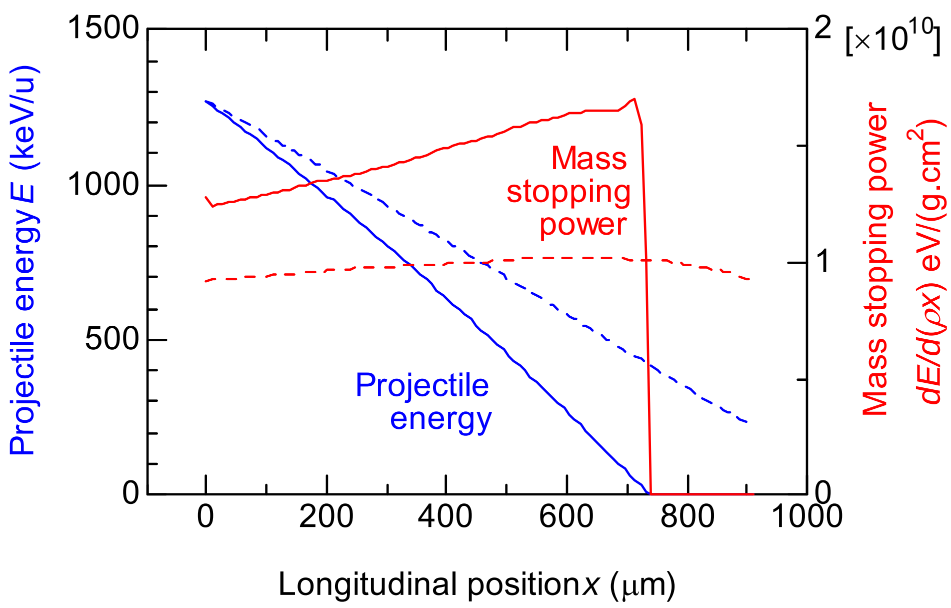

Linear decrease of *kT* near the exit of the target is due to the temporal change of the projectile range.

- Temporal evolution of the depth profile of temperature and specific energy deposition:
  - After t = 0.5 ns, projectile stops in the target.
  - The projectile range decreases with time for t > 0.5 ns.

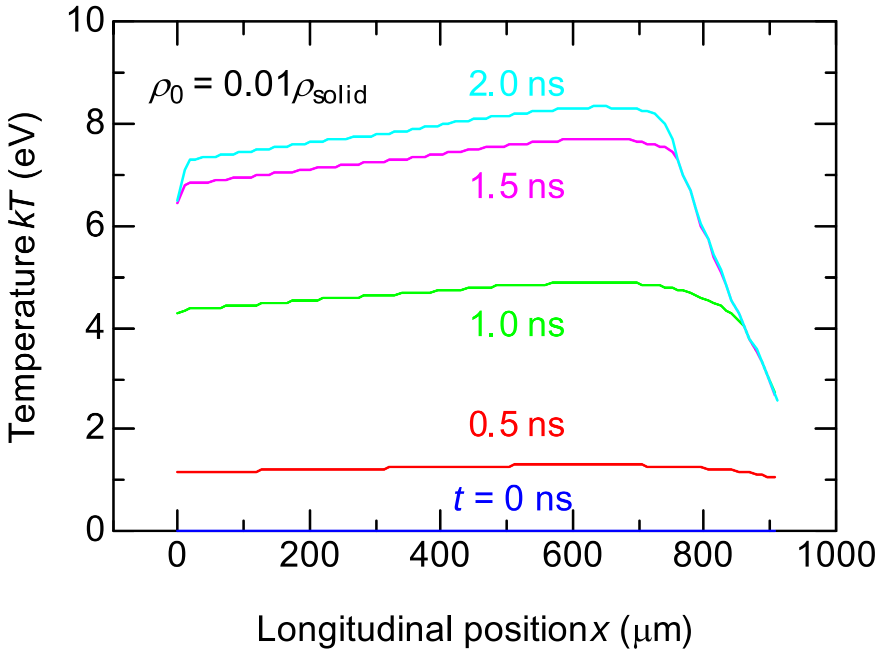

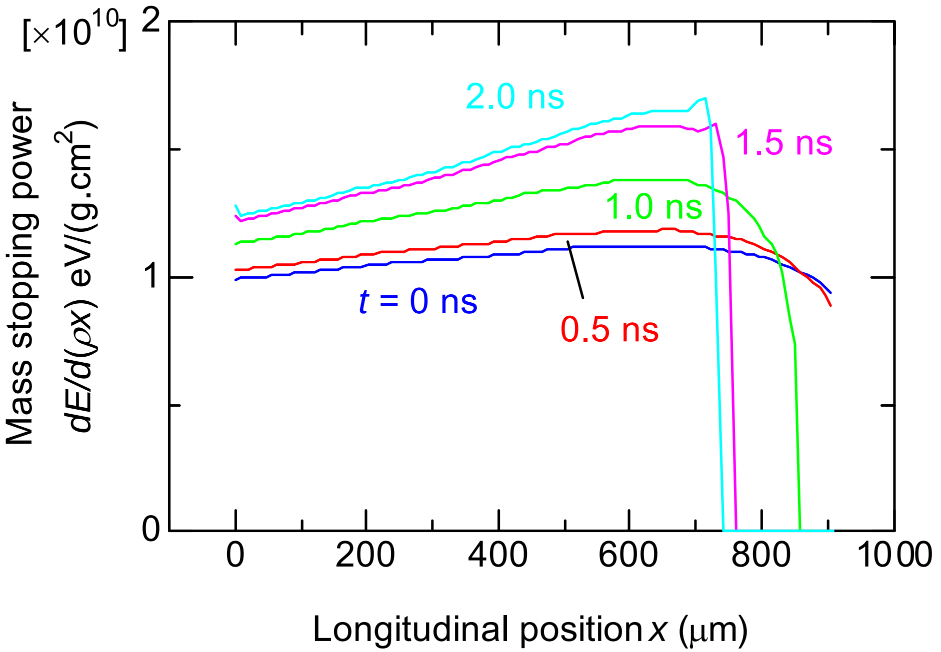

Temperature homogeneity can be improved simply by reducing the beam power.

- Snapshot of depth profile of kT and $dE/d(\rho x)$ at t = 2.0 ns (end of the pulse) for different beam fluxes:
- If the beam flux is reduced to 2 GW/mm^2,
  - the beam penetrates the target,
  - $dE/d(\rho x)$ inhomogeneity is ±26%,
  - the maximum temperature decreases to $kT \approx$ 3 eV.

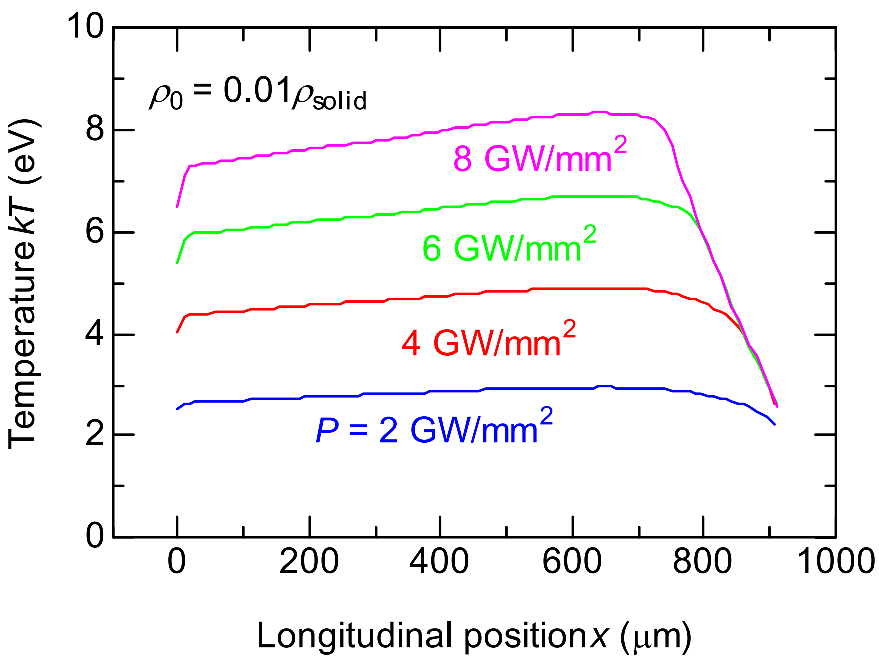

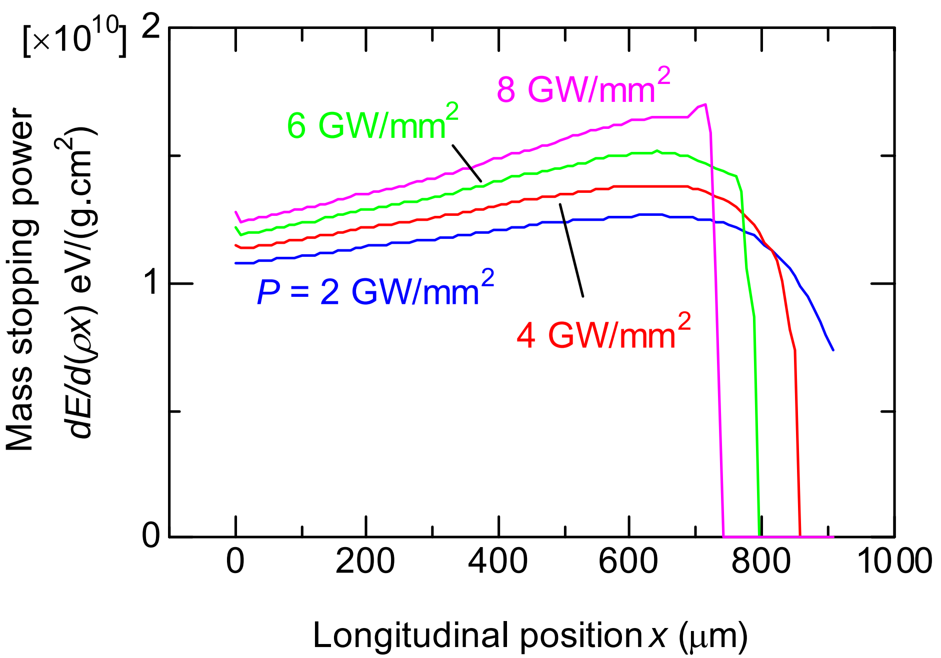

To simulate the inhomogeneous porous foam target, a multilayer target structure was investigated.

- Assumption for the $\rho = 0.01\rho_{\mathrm{solid}}$ foam structure:
  - Effective cell-wall thickness = 0.1 μm
  - Effective pore size = 10 μm
- Preliminary results:
  - P_{peak} = 8 GW/mm^2, τ = 1 ns

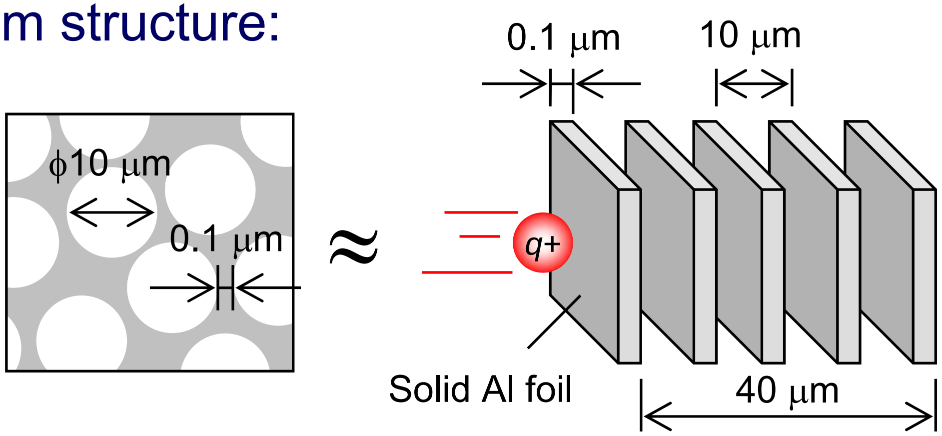

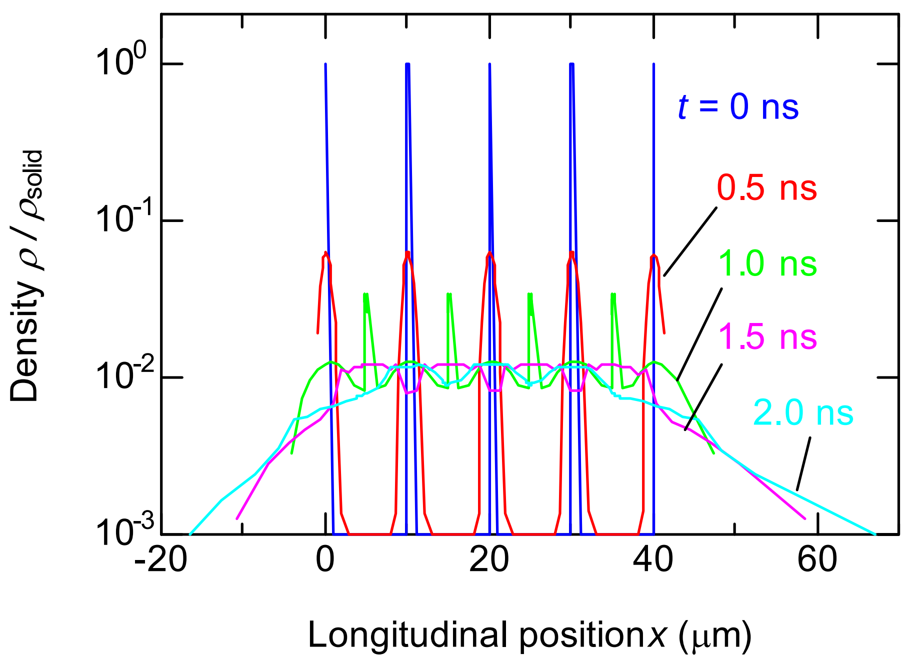

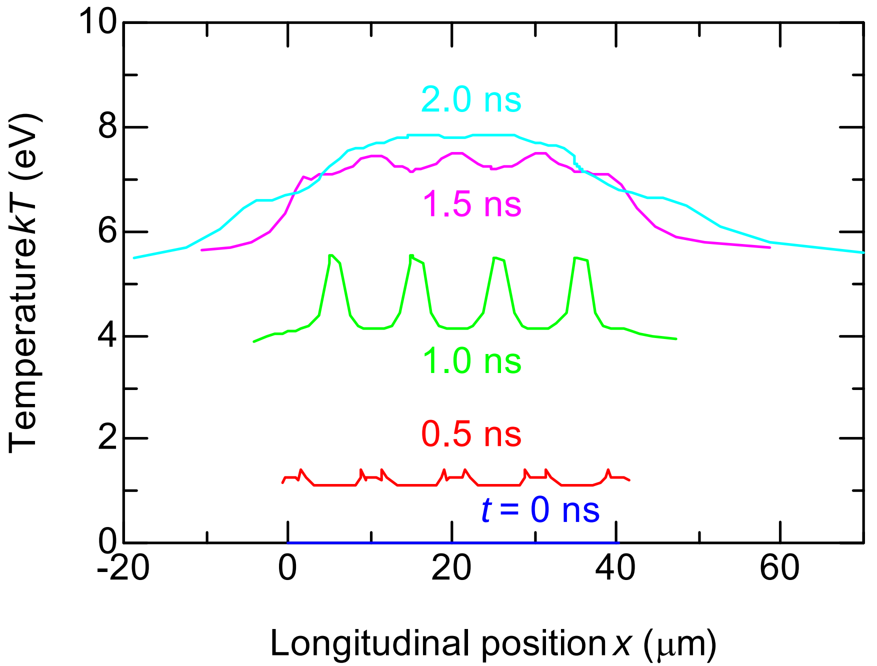

Conclusions: $dE/d(\rho x)$ data as a function of ρ and kT are important for detailed design of experimental setup.

- A numerical tool was developed to calculate heavy-ion stopping power in warm dense targets:
  - Energy loss of “Intermediate”-energy projectiles in targets with a given density and a given temperature can be calculated.
  - The shape of the calculated Bragg curve for cold targets agrees well with those on the well-established databases.
- The *dE/dx* code was successfully coupled to the 1D hydro code MULTI.
- Low-density foam target is necessary, but the sensitivity of $dE/d(\rho x)$ to change of kT and ρ may be strong!

Target ($_{18}$Al)		Effect of hydro expansion	Change of $dE/d(\rho x)$ by heating and expansion
Density	Geom. thickness		
High (≈ solid)	Thin (≈ 10 μm)	Large ☹	Small ☺
Low (foam)	Thick (≈ 1 mm)	Small ☺	Large ☹

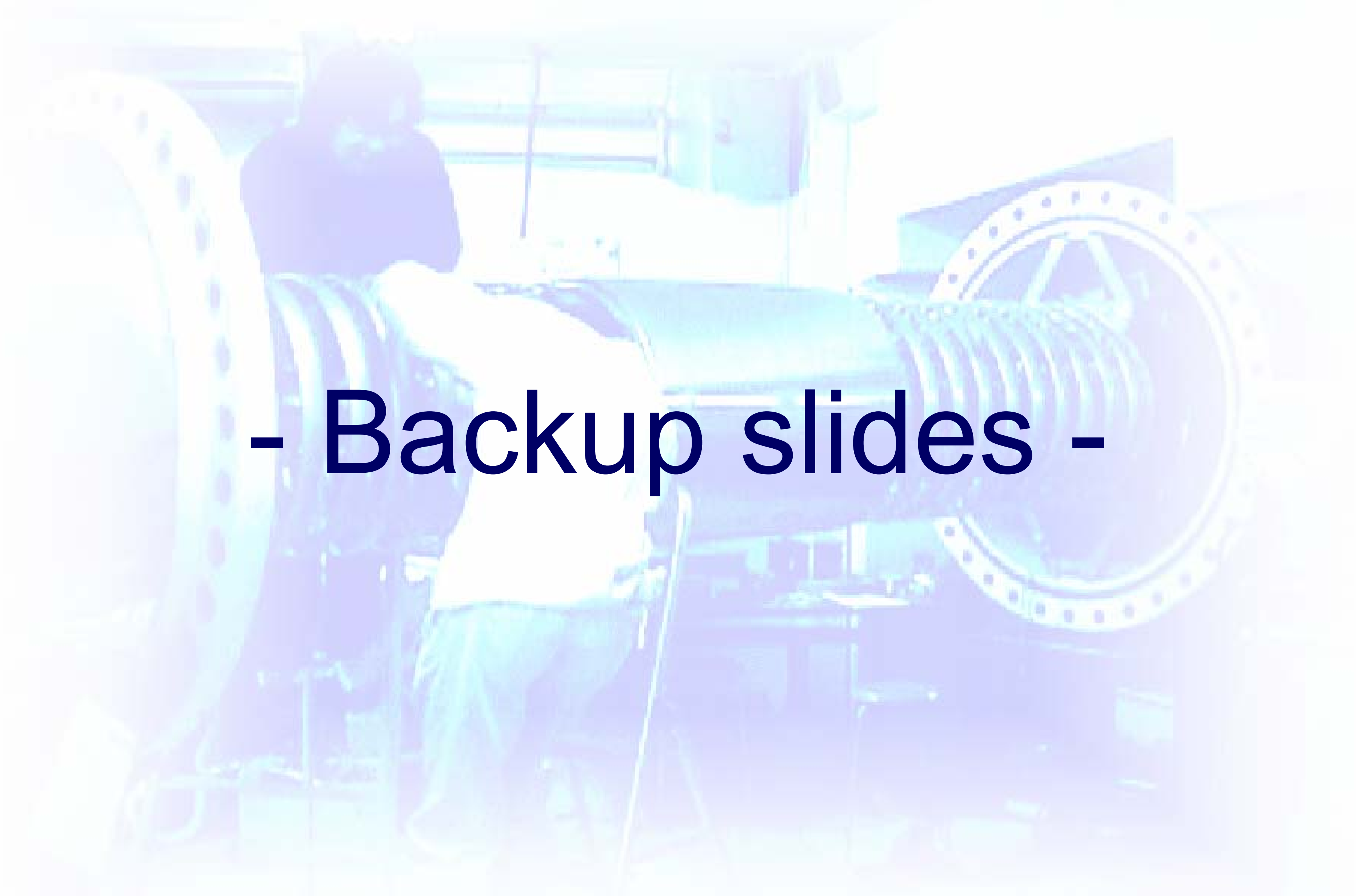

- Backup slides -

To check the validity of the present method, effect of solid-gas phase transition was examined.

- Example: Electron density- and velocity distribution in an Ar atom with sold- and gas phase:

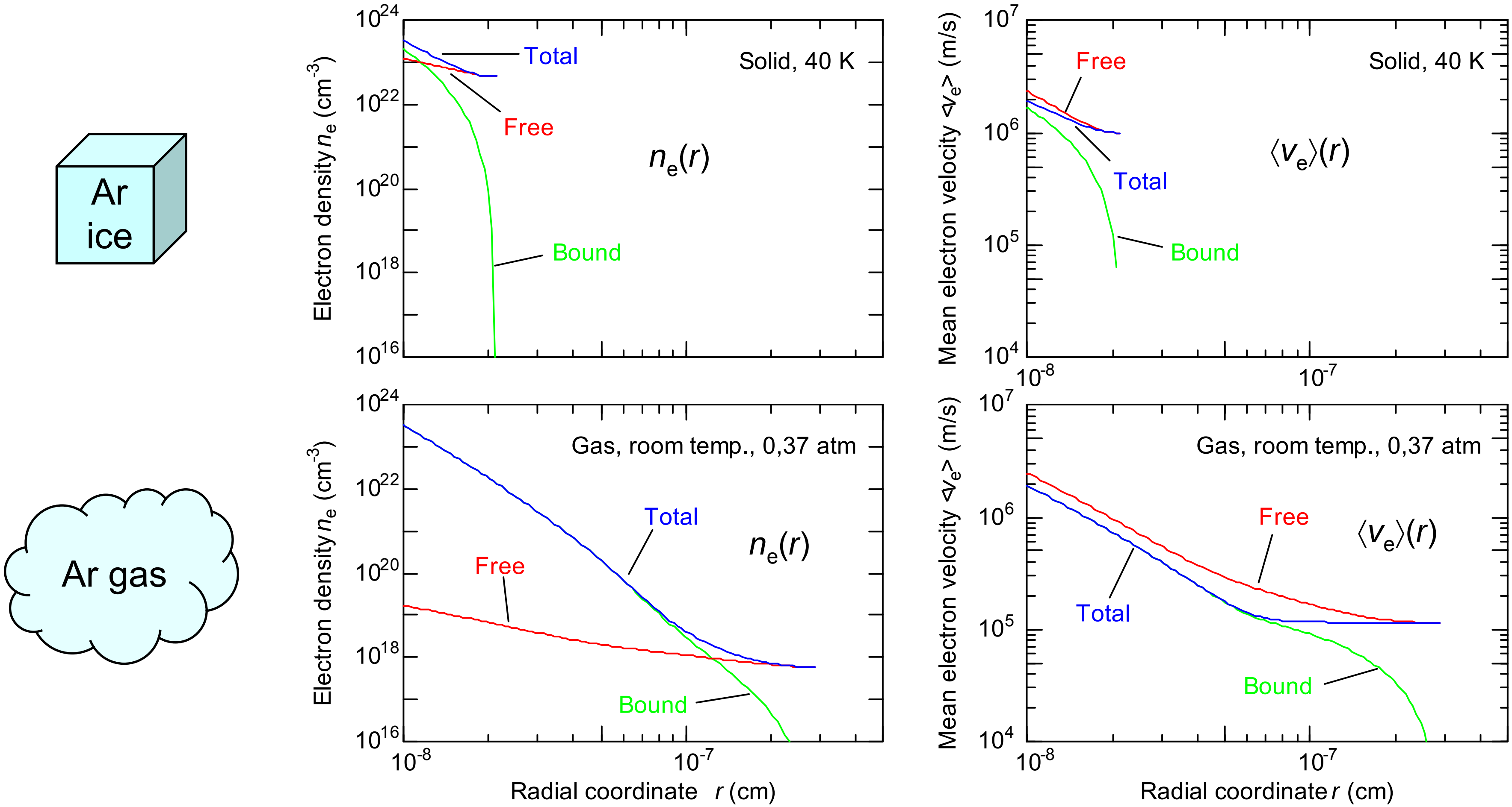

Calculated solid/gas ratio of $dE/d(\rho x)$ is roughly consistent with experimental results.

- Example: Stopping cross section of ^{4}He projectiles in gas / solid $_{18}$Ar:
  - Projectile effective charge was adjusted to fit to an established cold gas data.

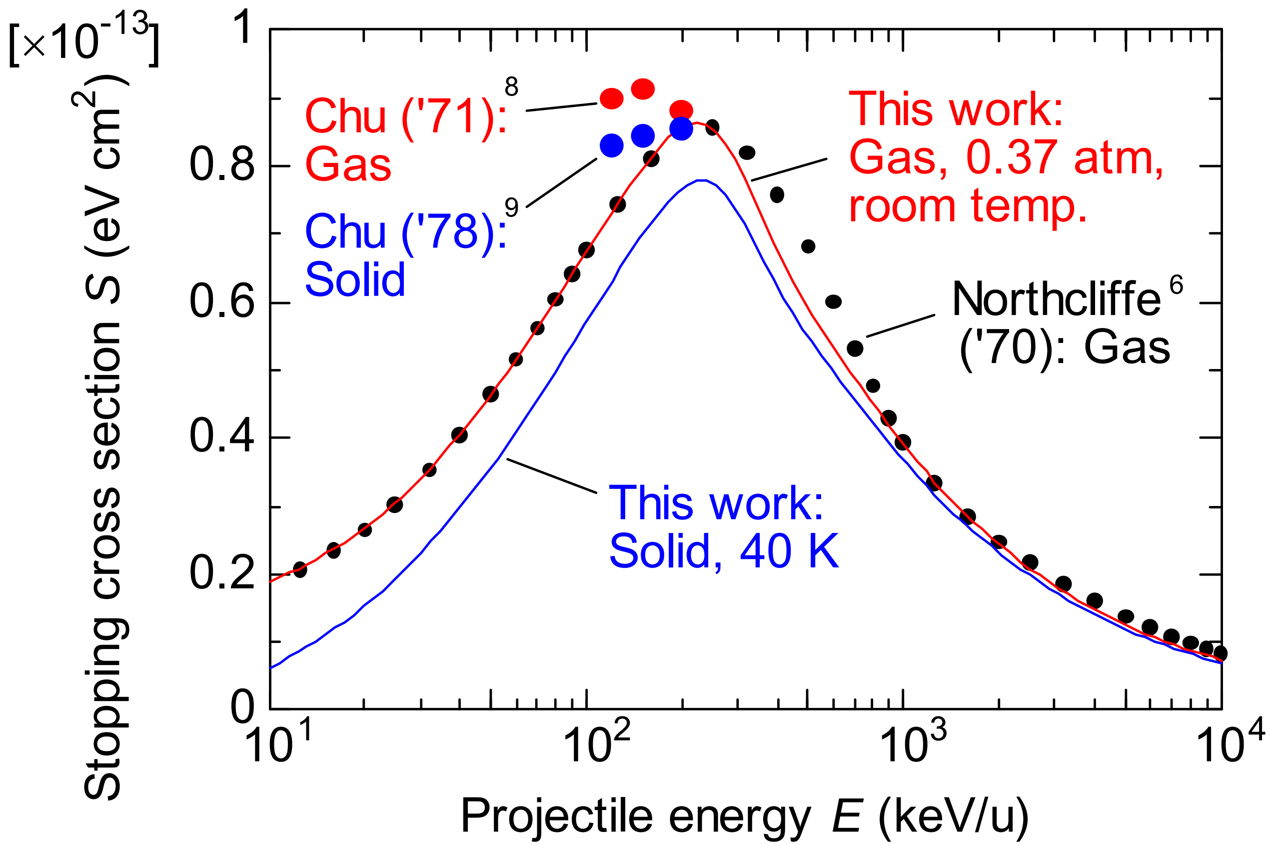

Argon ice

Melting point = 83.8 K
ρ_{solid} = 1.65 g/cm³ @ 40 K

[8]W. K. Chu et al., *Nucl. Instr. and Meth* **149** (1978) 115.
[9]W. K. Chu and D. Powers, *Phys. Rev.* B **4** (1971) 10.

High sensitivity of *dE/dx* to *kT* at low densities is due maybe to high ionization degree of the target.

- Comparison of Z_{ion} ($\propto$ ionization degree) on different EOS data:
  - Thomas-Fermi calculation in this work yields exactly same Z_{ion} as MPQOES[10] table, which is based on QEOS[11].
  - MPQEOS exhibits higher Z_{ion} than SESAME.

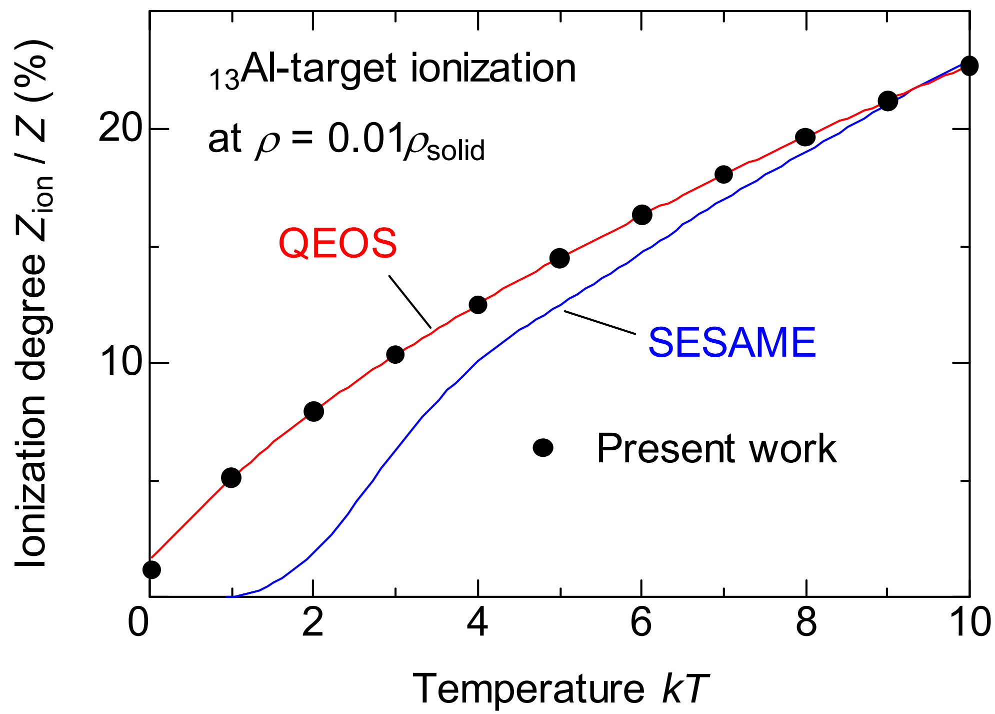

[10]A. Kemp and J. Meyer-ter-Vehn, *Nucl. Instr. and Meth.* A **415** (1998) 674.
[11]R. More et al. *Phys. Fluids* **31** (1988) 3059.

“Warm” hydrogen target is available by using an electromagnetically-driven shock tube at Tokyo Tech.

- Phase transitions:
  - Dissociation of molecules
  - Excitation of neutral atoms
  - Ionization
- By adjusting the shock speed, almost pure atomic ground-state target will be available:
  - Atomic density $\approx 10^{18}$ cm^{-3} ($p_0(H_2)$ = 9 Torr)
  - Temperature = 0.5 eV
  - Ionization < 0.1%
  - Very small fraction of excited states

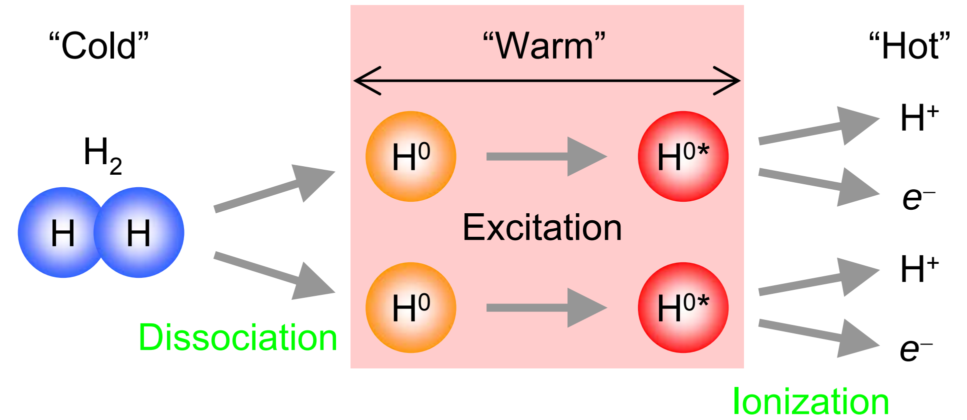

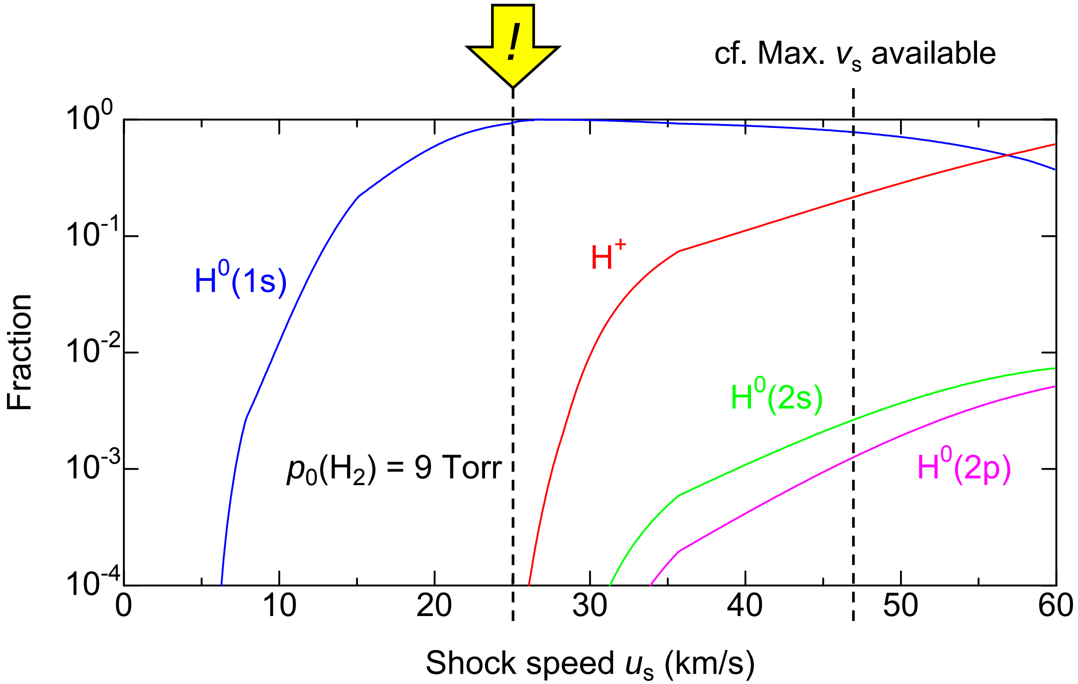

Energy of single ions after passage through the atomic target was measured by a solid-state detector.

- The beam deflector has to be synchronized to the shock wave:

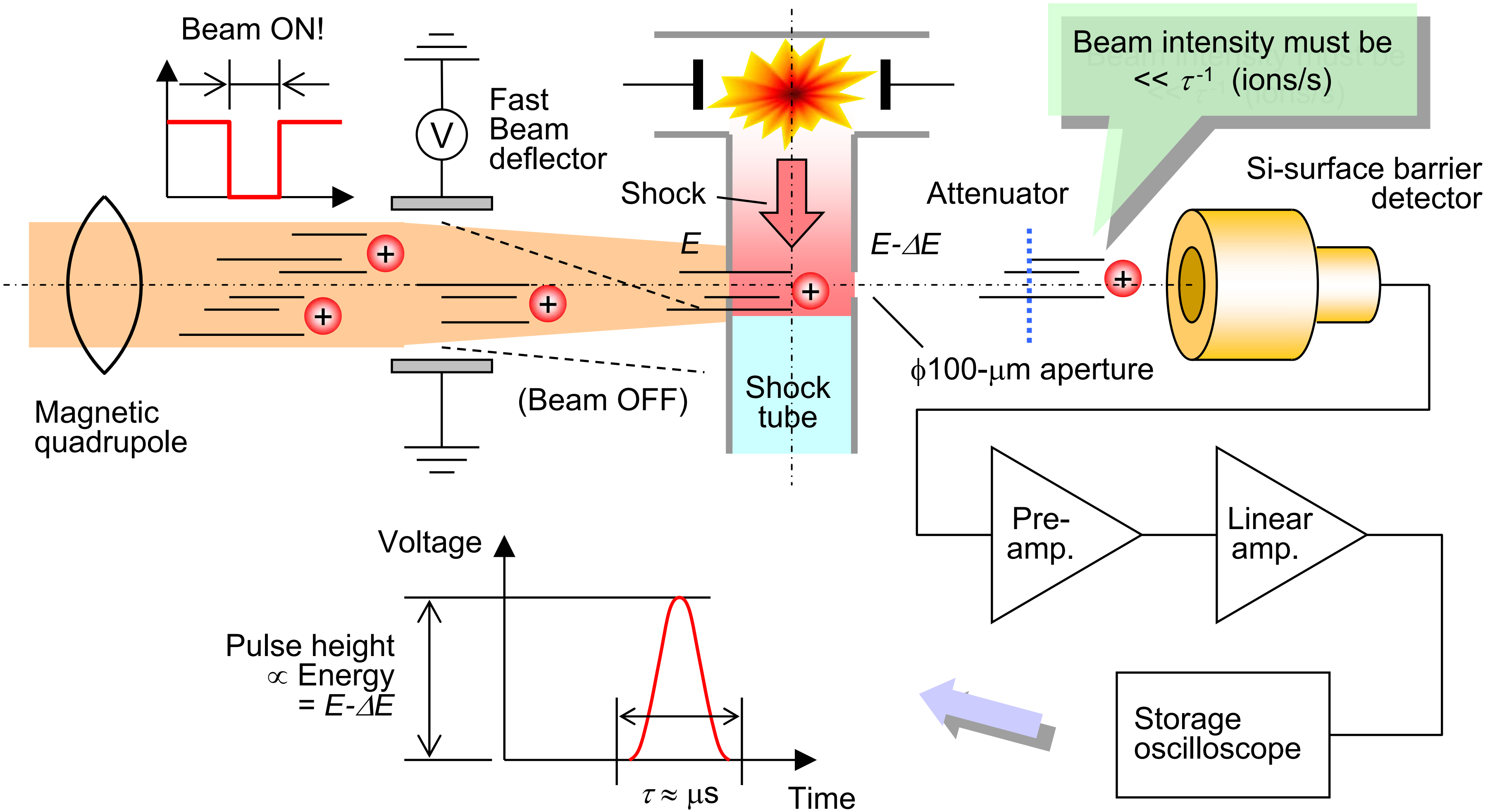

Experimental error should be reduced to clearly show the effect of dissociation of the target.

- Preliminary experimental result on the stopping cross section of ^{12}C projectiles in a dissociated atomic hydrogen target:
  - Solid lines: numerical results (energy transfer by binary collision, projectile charge-state determined by electron loss/capture cross sections)

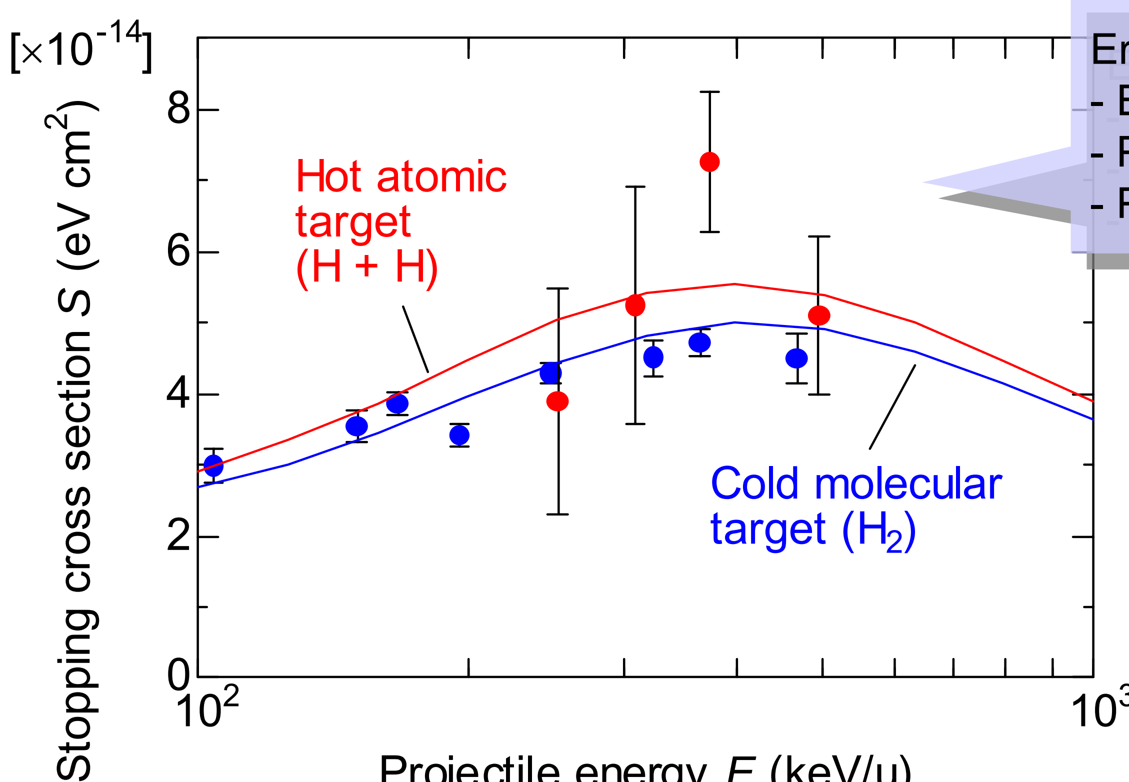

Error is due to:
- Electric discharge noise
- Plasma light noise
- Poor reproducibility of target

The electron phase space distribution $f_e(r,v_e)$ has been determined by an iterative calculation.

- Relations between electric potential $\phi(r)$, electron density $n_e(r)$ and Fermi energy E_F in a Thomas-Fermi model:
  - $\phi(r)$ can be calculated using $n_e(r)$ and Z by

$$\phi(r)=\frac{1}{4\pi\varepsilon_0}\left(\frac{Ze}{r}-\int_{r=0}^{R_{WS}}\frac{en_e(r)}{|r-r'|}dr^3\right).$$

  - $n_e(r)$ is recursively given by

$$n_e(r)=\int_0^\infty f_e(r,p)dp=n_{eb}(r)+n_{ef}(r).$$

  - E_F can be determined by the charge neutrality:

$$\int_0^{R_{WS}} n_e(r)dr^3=Z.$$

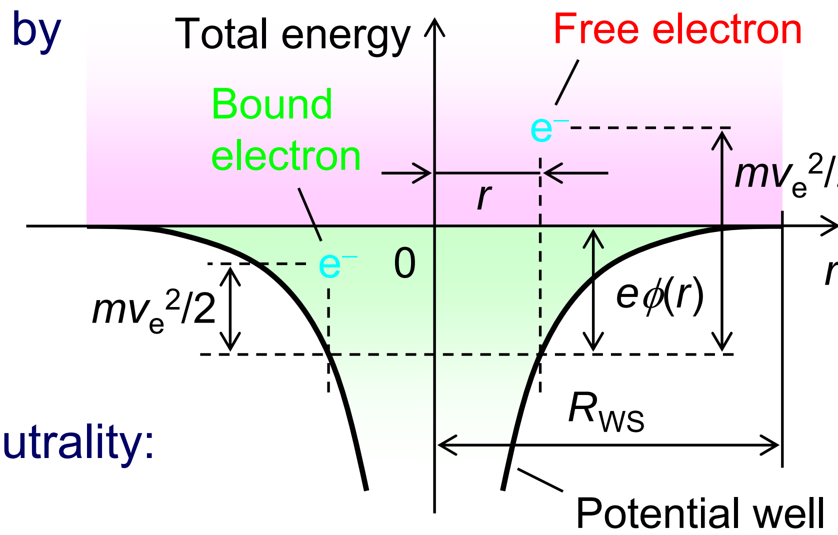

  - Bound-electron component:

$$n_{eb}(r)=\int_0^{\sqrt{2e\phi(r)/m}} f_e(r,v_e)dv_e \qquad \langle v_{eb}\rangle(r)=\left(\int_0^{\sqrt{2e\phi(r)/m}} v_e^2 f_e(r,p)dv_e\right)^{1/2}$$

  - Free-electron component:

$$n_{ef}(r)=\int_{\sqrt{2e\phi(r)/m}}^{\infty} f_e(r,v_e)dv_e \qquad \langle v_{ef}\rangle(r)=\left(\int_{\sqrt{2e\phi(r)/m}}^{\infty} v_e^2 f_e(r,v_e)dv_e\right)^{1/2}$$

Position and height of Bragg-peak can change with physical/chemical condition of the target material.

- For fixed projectile charge q, $-dE/dx$ is maximum at projectile velocity $v_p \approx v_e$:

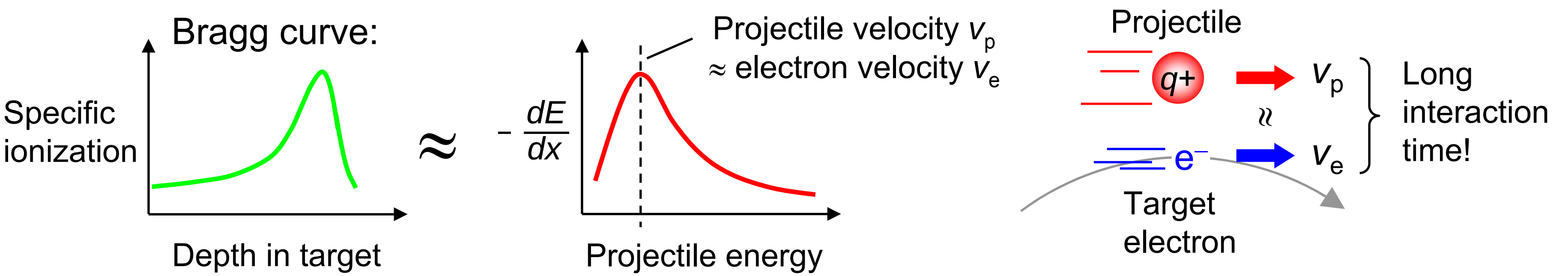

- Target electron velocity v_e (kinetic energy) changes with target conditions:
  - Physical phase (solid, liquid, gas, WDM, plasma, ……)
  - Chemical state (single atom, compound, crystal, ……)
  - Density (pressure), temperature

→ Bragg peak position/height can change!